Quaternary Science Reviews 160 (2017) 116–137

Contents lists available at ScienceDirect

Quaternary Science Reviews

journal homepage: www.elsevier.com/locate/quascirev

Deglacial variability in Okhotsk Sea Intermediate Water ventilation and biogeochemistry: Implications for North Pacific nutrient supply and productivity

Lester Lembke-Jene [a, *], Ralf Tiedemann [a], Dirk Nürnberg [b], Ulla Kokfelt [c], Reinhard Kozdon [d], Lars Max [a], Ursula Röhl [e], Sergey A. Gorbarenko [f]

[a] Alfred-Wegener-Institut Helmholtz-Zentrum für Polar- und Meeresforschung, Am Handelshafen 12, 27570 Bremerhaven, Germany
[b] GEOMAR Helmholtz-Zentrum für Ozeanforschung, Am Seefischmarkt 1-3, 24148 Kiel, Germany
[c] GEUS, Geological Survey of Denmark and Greenland, Øster Voldgade 10, 1350 Købnhaven, Denmark
[d] Lamont-Doherty Earth Observatory, Columbia University, Palisades, NY, USA
[e] MARUM Center for Marine Environmental Sciences, University of Bremen, Leobener Strasse, 28359 Bremen, Germany
[f] V.I. Il'ichev Pacific Oceanological Institute FEB-RAS, Baltijskaja Str. 43, RU-690041 Vladivostok, Russia

ARTICLE INFO

Article history:
Received 10 February 2016
Received in revised form
16 January 2017
Accepted 25 January 2017
Available online 17 February 2017

Keywords:
North Pacific
Paleoceanography
Glacial termination
Intermediate water
Bio-productivity
Okhotsk sea
Biological pump
Siberian hinterland
Stable isotopes
Subarctic gyre

ABSTRACT

The modern North Pacific plays a critical role in marine biogeochemical cycles, as an oceanic sink of CO_2 and by bearing some of the most productive and least oxygenated waters of the World Ocean. The capacity to sequester CO_2 is limited by efficient nutrient supply to the mixed layer, particularly from deeper water masses in the Pacific's subarctic and marginal seas. The region is in addition only weakly ventilated by North Pacific Intermediate Water (NPIW), which receives its characteristics from Okhotsk Sea Intermediate Water (OSIW). Here, we present reconstructions of intermediate water ventilation and productivity variations in the Okhotsk Sea that cover the last glacial termination between eight and 18 ka, based on a set of high-resolution sediment cores from sites directly downstream of OSIW formation. In a multi-proxy approach, we use total organic carbon (TOC), chlorin, biogenic opal, and $CaCO_3$ concentrations as indicators for biological productivity. C/N ratios and XRF scanning-derived elemental ratios (Si/K and Fe/K), as well as chlorophycean algae counts document changes in Amur freshwater and sediment discharge that condition the OSIW. Stable carbon isotopes of epi- and shallow endobenthic foraminifera, in combination with ^{14}C analyses of benthic and planktic foraminifera imply decreases in OSIW oxygenation during deglacial warm phases from c. 14.7 to 13 ka (Bølling-Allerød) and c. 11.4 to 9 ka (Preboreal). No concomitant decreases in Okhotsk Sea benthic-planktic ventilation ages are observed, in contrast to nearby, but southerly locations on the Japan continental margin. We attribute Okhotsk Sea mid-depth oxygenation decreases in times of enhanced organic matter supply to maxima in remineralization within OSIW, in line with multi-proxy evidence for maxima in primary productivity and supply of organic matter. Sedimentary C/N and Fe/K ratios indicate more effective entrainment of nutrients into OSIW and thus an increased nutrient load of OSIW during deglacial warm periods. Correlation of palynological and sedimentological evidence from our sites with hinterland reference records suggests that millennial-scale changes in OSIW oxygen and nutrient concentrations were largely influenced by fluvial freshwater runoff maxima from the Amur, caused by a deglacial northeastward propagation of the East Asian Summer Monsoon that increased precipitation and temperatures, in conjunction with melting of permafrost in the Amur catchment area. We suggest that OSIW ventilation minima and the high lateral supply of nutrients and organic matter during the Allerød and Preboreal are mechanistically linked to concurrent maxima in nutrient utilization and biological productivity in the subpolar Northwest Pacific. In this scenario, increased export of nutrients from the Okhotsk Sea during deglacial warm phases supported subarctic Pacific shifts from generally Fe-limiting conditions to transient nutrient-replete

* Corresponding author.
E-mail addresses: lester.lembke-jene@awi.de (L. Lembke-Jene), ralf.tiedemann@awi.de (R. Tiedemann), dnuernberg@geomar.de (D. Nürnberg), ulk@geus.dk (U. Kokfelt), rkozdon@ldeo.columbia.edu (R. Kozdon), lars.max@awi.de (L. Max), uroehl@marum.de (U. Röhl), gorbarenko@poi.dvo.ru (S.A. Gorbarenko).

http://dx.doi.org/10.1016/j.quascirev.2017.01.016

regimes through enhanced advection of mid-depth nutrient- and Fe-rich OSIW into the upper ocean. This mechanism may have moderated the role of the subarctic Pacific in the deglacial CO_2 rise on millennial timescales by combining the upwelling of old carbon-rich waters with a transient delivery of mid-depth-derived bio-available Fe and silicate.

1. Introduction

Today, no new deepwater is formed in the subarctic North Pacific, because the surface water masses are not dense enough to sink to significant water depths and initiate convection due to low surface salinities and an associated strong halocline (Emile-Geay et al., 2003; Warren, 1983). Accordingly, the deep North Pacific is only weakly ventilated and carries high concentrations of macronutrients, in particular nitrate and silicate. In contrast, the intermediate-depth level is occupied by a relatively fresh and oxygen-enriched layer of North Pacific Intermediate Water (NPIW, Reid, 1965; Talley, 1993). NPIW is today mainly characterized through a ventilated precursor water mass, the Okhotsk Sea Intermediate Water (OSIW, Watanabe and Wakatsuchi, 1998). Modern NPIW and OSIW are highly variable in their biogeochemical characteristics, even on relatively short (i.e. multi-decadal) instrumental timescales (Emerson et al., 2004; Tadokoro et al., 2009), and keep mid-depth waters in the North Pacific moderately oxygenated. While the North Pacific overall is a large modern oceanic sink for atmospheric CO_2 (Takahashi et al., 2009), surface utilization of nutrients by primary producers and export production of carbon (the "biological pump") remains incomplete in the Western Subarctic Pacific (WSAP) Gyre, mainly due to the rapid seasonal depletion of iron (Fe) as micronutrient (see review by Takeda, 2011), and silicate ($Si(OH)_4$; Harrison et al., 2004). On glacial-interglacial timescales the export production and degree of surface nutrient utilization, as evidenced by studies of $\delta^{15}N$, are anti-correlated, implying more effective use of available nutrients during glacial periods (e.g. Galbraith et al., 2008; Jaccard et al., 2005). This more effective utilization allowed a lower primary production to export carbon from the surface into the deep ocean more efficiently. Thus, indicators for export production varied in phase with atmospheric CO_2 concentrations for at least the last 800 ka (Jaccard et al., 2010).

However, on shorter, millennial timescales this relatively straightforward relation does not necessarily hold. During the last glacial termination, surface nutrient utilization and export production become partially decoupled in the WSAP (Brunelle et al., 2010; Kohfeld and Chase, 2011; Maier et al., 2015). During the deglacial warm Bølling-Allerød (B-A) and Preboreal (PB) phases, widespread productivity peaks were accompanied by more effective nutrient utilization, contrary to glacial-interglacial patterns (Kohfeld and Chase, 2011). Such millennial-scale structures call for additional mechanisms that regulate the nutrient dynamics in the mixed layer and their biological utilization. Potential candidates are changes in the ratio of macronutrients relative to bio-available iron (Brunelle et al., 2010; Kienast et al., 2004; Kohfeld and Chase, 2011) and changes in the physical stratification of the mixed layer (Lam et al., 2013; Riethdorf et al., 2013). In line with these deglacial changes in upper ocean processes, the North Pacific underwent drastic and rapid changes in intermediate to deep water circulation and ventilation (Duplessy et al., 1989; Okazaki et al., 2010), which are as well thought to being closely linked with changes in the utilization of nutrients and biogeochemistry (Crusius et al., 2004; Galbraith et al., 2007; Gebhardt et al., 2008). During the cold Heinrich Stadial 1 (HS-1, 17.5–15.0 ka), convection and the increased formation of new intermediate–deep water masses (down to 2800 m water depth) were proposed for the North Pacific (Okazaki et al., 2010), although newer evidence alternatively suggested that a potential Pacific overturning cell did not extend beyond 1400–2000 m water depth and was initiated through increased mid-depth ventilation in the marginal subarctic seas (Jaccard and Galbraith, 2013; Max et al., 2014; Okazaki et al., 2014). This early deglacial episode is sharply contrasted by subsequent oxygen declines in intermediate water depths during the B-A (14.7–12.9 ka) the PB, leading to widespread anoxia along the North American Pacific margins (Dean et al., 2006; Van Geen et al., 2003; Zheng et al., 2000), in the Bering Sea (Cook et al., 2005; Itaki et al., 2012; Kuehn et al., 2014), and on the western Pacific margin off Japan (Ikehara et al., 2006; Sagawa and Ikehara, 2008). In the pelagic abyssal North Pacific, no Oxygen Minimum Zones (OMZs) developed during this time (Jaccard and Galbraith, 2011; Jaccard et al., 2009). To explain the unusually severe and widespread O_2-depletion of intermediate waters during the Bølling-Allerød and Preboreal, increases in export production have been invoked (Davies et al., 2011; McKay et al., 2004; Mix et al., 1999). Alternatively, reduced or ceased ventilation of NPIW could have decreased O_2 concentrations across the North Pacific. (e.g. Duplessy et al., 1989; Keigwin et al., 1992; Zheng et al., 2000), or a combination of these processes was responsible for the decline in mid-depth O_2 concentrations by increased respiration of organic matter (OM) in initially well-ventilated NPIW, along its pathway in the Pacific (Crusius et al., 2004).

Previous works from the Okhotsk Sea and Bering Sea have shown that mixed layer stratification, sea ice action and export production varied on millennial timescales during the deglaciation, implying a combination of these potential factors, in addition to changes of freshwater runoff and the flooding of continental shelf areas by sea level rise (Gorbarenko, 2007a, 2008, 2012; Harada et al., 2008; Harada et al., 2012; Riethdorf et al., 2013). However, information used to infer changes often stemmed from single site locations, sometimes relatively distant to source regions of water formation processes or were affected by insufficient temporal resolution. In this study, we analyzed a suite of high-resolution sediment cores (with sedimentation rates between 20 and 200 cm/ka) retrieved directly downstream of the main ventilation region of OSIW, on the eastern continental margin of Sakhalin island in the Okhotsk Sea. We use a multi-proxy approach to discuss changes in ventilation and export production within the Okhotsk Sea as the most prominent modern NPIW ventilation source region. We put these outcomes into context with XRF-scanning based qualitative assessments of terrigenous supply of Fe as essential micro-nutrient and compare our results with earlier, published data that showed millennial-scale variations in ventilation and nutrient utilization during the last glacial termination (18–8 ka). We constrain potential causes for the observed rapid changes in OSIW/NPIW ventilation and productivity patterns, and assess their potential consequences for open-ocean WSAP nutrient supply and biogeochemistry.

2. Setting and modern hydrography

North Pacific Intermediate Water (NPIW) is defined as a salinity and potential vorticity minimum and spreads between the density lines of c. σ_Θ 26.6–27.2 (corresponding to c. 600–800 m water depth) east- and southward across the north Pacific down to a latitude of about 20° N (Fig. 2, Talley, 1993; Yasuda et al., 1996). Because water masses with these densities are at present not outcropping on the surface in the open North Pacific, NPIW is ventilated by one of its main precursor water mass, the Okhotsk Sea Intermediate Water (OSIW), through largely diapycnal mixing processes (Kitani, 1973; Shimizu et al., 2004). The principal origin for high O_2 of OSIW is Dense Shelf Water (DSW). At present, relatively warm WSAP Water is transported in the East Kamchatka Current southward as part of the larger Western Subarctic Pacific Gyre and enters the Okhotsk Sea mainly via Kruzensthern Strait and Bussol' Strait (Fig. 1). WSAP Water flows within the main cyclonic Okhotsk Gyre to the shallow northeastern shelf areas, where DSW is formed during the sea ice season north of Sakhalin by brine rejection in large persistently recurring polynias (Fukamachi et al., 2009; Shcherbina et al., 2004). DSW is characterized by relatively low salinity, very low temperatures and high O_2 content, and is subsequently entrained into deeper water layers along the northern Sakhalin margin by vertical tidal and diapycnal mixing while being transported by the East Sakhalin Current (ESC). It finally leaves the Okhotsk Sea as OSIW through deep passages (mainly Bussol' Strait) between the Kuril Islands and is transported with the Oyashio Western Boundary Current into the Mixed Water Region and the Western Pacific Subarctic Gyre circulation (Fig. 1, Shcherbina et al., 2004). This well ventilated, cold, low salinity OSIW (relative to NPIW) and the subsequent export of this water mass into the open North Pacific is critical for maintaining sufficiently high O_2 levels in the intermediate water layer of the extratropical North Pacific. Below the layer of OSIW, the Okhotsk Sea has a weakly developed OMZ today along the Sakhalin margin between ca. 1000 and 1400 m (Bubenshchikova et al., 2010; Nakatsuka et al., 2004a).

Not only does OSIW ventilate the intermediate-depth North Pacific, it also transports high amounts of both dissolved and particulate terrigenous matter along the Sakhalin margin into the open North Pacific within a turbid layer that bears extremely high concentrations of organic carbon, lithogenic particles, silicate and other suspended material (Hansell, 2002; Nakatsuka et al., 2004b). This material is entrained by vigorous tidal mixing on the northeastern shallow continental shelf into the turbid water layer and transported along the Sakhalin margin on the density surfaces of OSIW (Fig. 2) for long distances (Nakatsuka et al., 2004b). The remnants of this entrainment are visible in the pelagic subarctic North Pacific as intermediate maxima in both Dissolved and Particulate Organic Carbon (DOC and POC) (Goes et al., 2004; Hansell, 2002). In addition, a subsurface to intermediate-depth concentration maximum has been identified in both dissolved and particulate iron (Fe) in the North Pacific (Nishioka et al., 2003, 2007). Its origin was tracked to the Okhotsk Sea, where Fe is entrained both from surface sediments by tidal currents and surface river runoff during intense mixing processes on the shallow northern shelf areas into DSW/OSIW and is transported with OSIW into the open North Pacific (Nishioka et al., 2007; Takeda, 2011). The amount of Fe flux to the North Pacific surface water by OSIW and NPIW today is substantial. Results from time-series and modeling studies suggest that it is comparable to the modern Fe flux derived from long-range atmospheric dust transport (Nishioka et al., 2011), which has been conventionally regarded as the major delivery mechanism of Fe to the surface North Pacific to relieve micronutrient limitation (Duce and Tindale, 1991; Mahowald et al., 2005). Thus, the Okhotsk Sea also acts as a modern potential source region for both micronutrients, organic matter and macronutrients to distal pelagic regions in the western North Pacific (Misumi et al., 2011; Nishioka et al., 2011; Yamashita et al., 2010). During wintertime wind-induced deep mixing both soluble and particulate Fe are transported into the subsurface and surface water layer, where they become bio-available and induce additional wintertime extensive phytoplankton blooms in this Fe-micronutrient-limited High Nutrient - Low Chlorophyll (HNLC) region, effectively replenishing depleted stocks of atmospherically-derived Fe (Lam and Bishop, 2008; Misumi et al., 2011; Nishioka et al., 2011).

3. Materials and methods

3.1. Core locations, sediment properties

We use three sediment cores in this study (Fig. 1): gravity core LV29-79-3 (core 79 hereafter, 1082 m water depth), gravity core LV28-4-4 (core 4 hereafter, 674 m water depth and piston core SO178-13-6 (core 13 hereafter, 713 m water depth) were recovered onthe northeast Sakhalin continental margin from undisturbed, continuous hemipelagic sediment sequences in a number of expeditions with R/V *Akademik M. A. Lavrentiev* and R/V *Sonne* carried out within the framework of the bilateral Russian–German KOMEX projects between 1998 and 2004 (Biebow and Hütten, 1999; Biebow et al., 2002; Dullo and Biebow, 2004). As the cores used here were retrieved from a principally dynamic sedimentary environment with relatively active bottom currents, significant care was taken to obtain undisturbed cores from continental margin sites along Sakhalin that were free of both underlying large-scale fault features, as well as small-scale sedimentary reworking or re-distribution events (Biebow and Hütten, 1999; Biebow et al., 2002; Dullo and Biebow, 2004; Ludmann and Wong, 2003; Wong et al., 2003). Extensive use was made of existing Russian bathymetric and seismic survey data, complemented by the use of high-resolution shallow sub-bottom profiling systems on expeditions LV29 and SO178 to exclude sites probably affected by sediment re-distribution (Biebow et al., 2002; Dullo and Biebow, 2004). In the case of the externally mounted sub-bottom profiling system SES2000DS during LV29, e.g. an average penetration depth of 20–30 m was achieved with a resolution of 25 cm or better, depending on pulse length and frequency. With a total of 860 km of profiles obtained, core 79 was retrieved from a facies with parallel, undisturbed high-amplitude reflectors with good continuity (Biebow et al., 2002). In the case of SO178, the shipboard Atlas Parasound sub-bottom profiling and SIMRAD 120 multibeam echosounder systems were used to search for and select sites for coring operations, in the course of which a total of more than 2000 nautical miles of bathymetric profiles were obtained (Dullo and Biebow, 2004). Like in previous expeditions, core 13 was retrieved from a flat, protected site with no indications of sediment re-working or disturbances. Details for survey lines shot across sites were given in the respective cruise reports (Biebow and Hütten, 1999; Biebow et al., 2002; Dullo and Biebow, 2004).

All cores feature similar lithofacies, consisting mainly of silty clays with sand and occasional larger dropstones derived from sea ice-transported terrigenous matter (Fig. 1, details Table S1). Cores were sampled with varying resolution between 2 and 20 cm, depending on the respective sample protocols for each expedition (cf. Biebow and Hütten, 1999; Biebow et al., 2002; Dullo and Biebow, 2004). In some cases such changing sampling protocols over the course of the years led to different sample resolutions depending on which proxies were used.

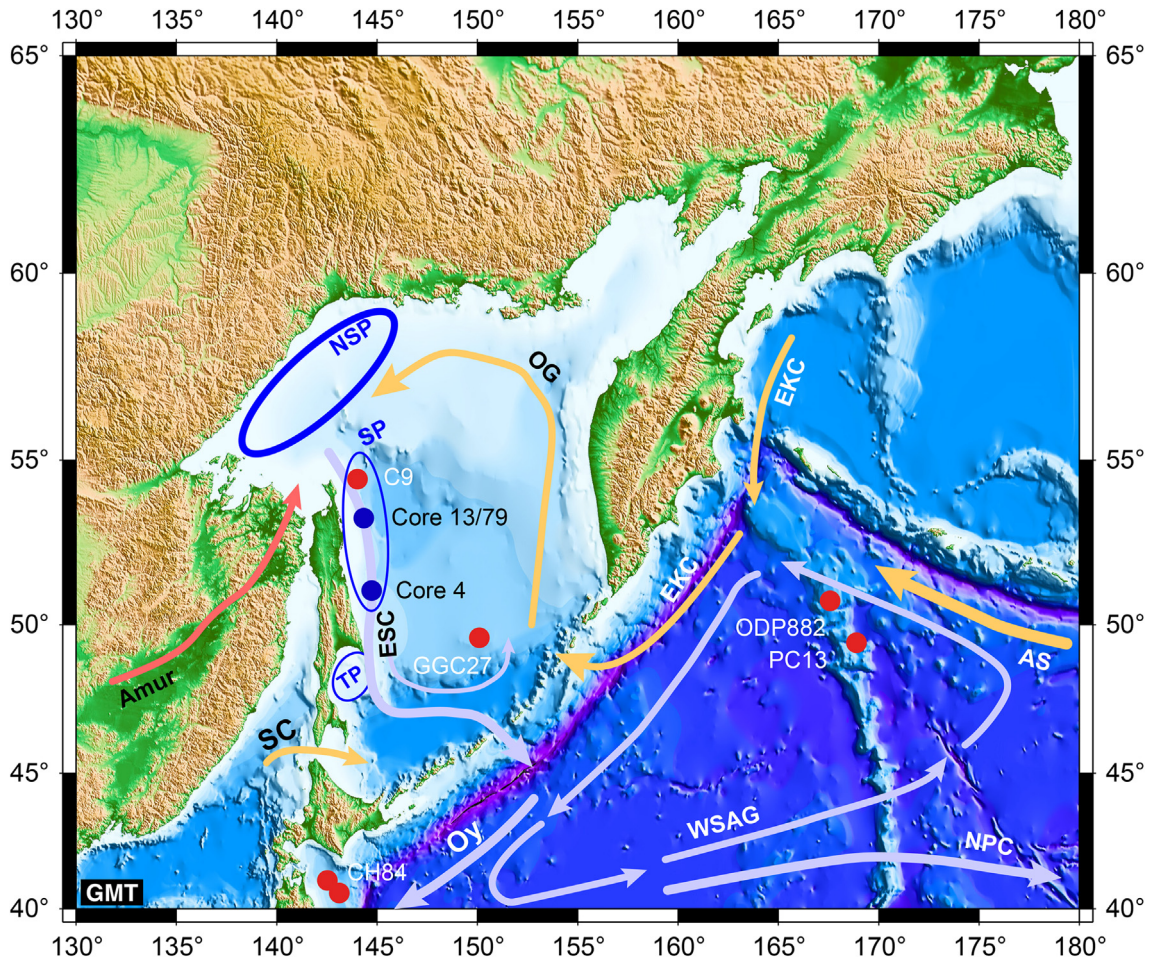

Fig. 1. Map of the NW Pacific study area. Core locations of this study marked as blue circles (see Table S1 for details), core locations of other studies used here as red filled circles. Major regional currents are outlined as arrows (yellow = relatively warmer, light blue = relatively colder) and abbreviated: Alaskan Stream (AS), East Kamchatka Current (EKC), Okhotsk Gyre (OG), Soya Warm Current (SC); East Sakhalin Current (ESC), Oyashio (Oy), Western Subarctic Gyre (WSAG) North Pacific Current (NPC). Red arrow indicates freshwater outflow by Amur into the NE Okhotsk Sea. The blue bold ellipse shows the major modern, recurring Northern Shelf Polynia (NSP) system; the smaller ellipses denote secondary systems: Sakhalin Polynia (SP), Terpeniya Bay Polynia (TBP). (For interpretation of the references to colour in this figure legend, the reader is referred to the web version of this article.)

3.2. AMS ^{14}C measurements

Age control was achieved through radiocarbon dating of planktic foraminifera, and benthic fauna in a few cases if the available samples did not yield enough foraminifera. For radiocarbon analyses *N. pachyderma* (s) and *G. bulloides* were picked from the 150–250 μm size fraction. Most radiometric dates were measured in the Leibniz Laboratory for Radiometric Dating and Isotope Research, Kiel according to established standard workflow protocols (Nadeau et al., 1997, 1998). Dating of two samples at a later stage was carried out by the W. M. Keck Carbon Cycle Accelerator Mass Spectrometry Laboratory at University of California, Irvine according to established protocols. Conventional ^{14}C ages are reported according to Stuiver and Polach (1977). To better assess changes in the ventilation of intermediate water masses we supplement our data with a set of deepwater ventilation ages derived from published data and measurements of planktic foraminifera and benthic organisms from the same core depths. We use raw Benthic-Planktic (or B-P) ages, expressed in ^{14}C years. This technique, while not without errors e.g. due to changing surface reservoir age changes has nonetheless been successfully used in a number of studies in this region before (e.g. Ahagon et al., 2003; Max et al., 2014; Okazaki et al., 2010). We do not use the alternative projection age method, as one of the underlying assumptions of this method, is the single-source origin of the originating water mass may be violated in this region of active water formation. The data used and their respective sources are listed in Supplementary Tables S2 and S3.

3.3. Stable isotope measurements

To deduce changes in the ventilation of OSIW we use stable isotopes of benthic foraminifera. The $\delta^{13}C$ of various epibenthic *Cibicidoides* species is widely used as reliable and well understood proxy for the $\delta^{13}C_{\sum CO2}$ and thus ventilation properties of bottom waters (e.g. McCorkle et al., 1997). These species have an epibenthic to slightly elevated epibenthic lifestyle (Lutze and Thiel, 1989). In addition, they exhibit relatively low tolerances against longer hypoxic periods in their environment and are often absent in OMZs in the Okhotsk Sea (Bubenshchikova et al., 2008). In the Okhotsk Sea, mainly two cibicid species have been found, *C. mundulus* and *C. lobatulus*. In this paper, we only use the former due to its more regular abundance in samples from all three cores and to obtain species-specific time series. This species has been shown to reliably record ambient average bottom water $\delta^{13}C$ of the dissolved inorganic carbon (DIC) in the Pacific

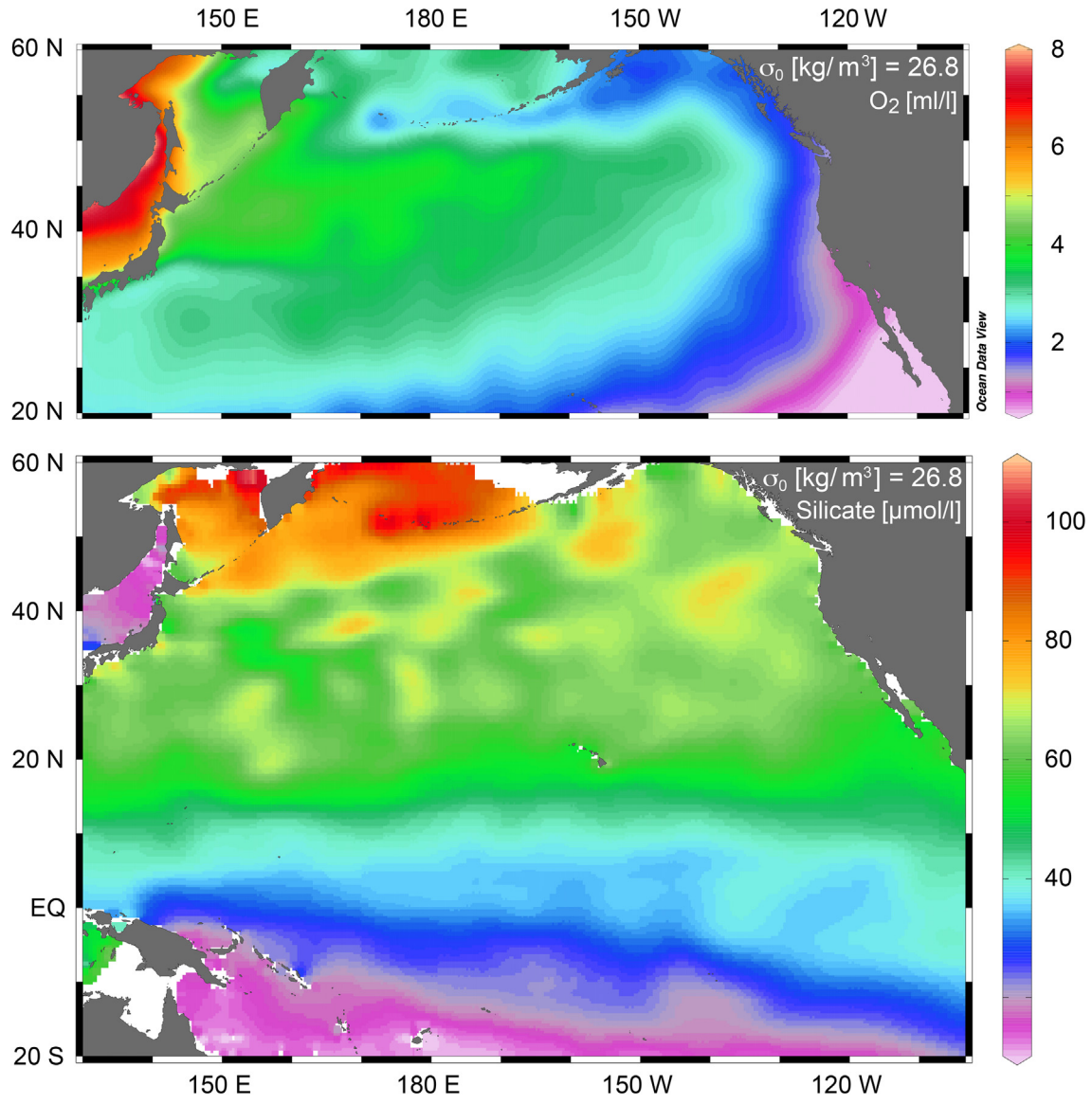

Fig. 2. Modern lateral distribution of (a) Oxygen in µmol/l and (b) Silicate in µmol/kg according to World Ocean Atlas 2009 data (Garcia et al., 2010a,b) along the main density surface of OSIW and NPIW at $\sigma_\Theta = 26.8$ kg/m^3. The software ODV (vers. 4.5.1) was used for visualization (Schlitzer, 2002).

region (McCorkle and Keigwin, 1994), even under high organic matter flux and deposition of phytodetritus layers on the sediment surface. In the Okhotsk Sea, subsurface and deeper water mass $\delta^{13}C_{DIC}$ is roughly linearly correlated with water column PO_4 and O_2 content (Bauch et al., 2002), and thus allows using $\delta^{13}C_{Cib}$ data as proxy for ventilation of OSIW. In addition, we analyzed samples of the species *Uvigerina peregrina* as qualitative indicator for sediment oxygenation and changes in pore water O_2 concentrations as a function of organic carbon flux. Sediment samples were weighed, freeze-dried and subsequently washed over a 63 µm screen. Dried samples were sieved into 63–150, 150–250, 500–1000, and >1000 µm fractions and weighed. Specimen for isotope analyses were picked from the 250–500 µm fraction, between one and five tests were used for each depth interval. All specimens were inspected for preservation; only well-preserved tests with translucent and non-corroded walls were used. Measured foraminifera were clean, did not show signs of re-crystallisation or overgrowths and had lustrous, unpitted test surfaces with open and original pores, as checked under light and scanning electron microscopy on selected samples. Foraminiferal abundances were principally low in all cores (as were carbonate concentrations in some intervals). In some samples, we were not able to find the desired species. Some clearly defined, limited intervals of the cores had indications of carbonate concretions and diagenesis detected in the shipboard sampling and description procedures (cf. Biebow and Hütten, 1999; Biebow et al., 2002; Dullo and Biebow, 2004). We avoided using samples from these intervals.

All stable isotope analyses were carried out in the Paleoceanography Stable Isotope Laboratory at GEOMAR, Kiel with a Thermo Finnigan MAT 252 mass spectrometer, coupled online to an automated Kiel II AUTO CARBO carbonate preparation device. Long-time analytical precision was better than ±0.08‰ for $\delta^{18}O$ and ±0.05‰ for $\delta^{13}C$. Calibration was achieved via an in-house Solnhofen limestone standard and National Institute of Standards (NIST) NBS-19. Results are reported in the δ notation as per mille with reference to Vienna - Pee Dee Belemnite (‰ V-PDB; Craig, 1957).

3.4. Productivity proxy records – chlorin, TOC, $CaCO_3$, opal

Productivity proxy analyses followed established procedures in the Sedimentology/Anorganic Geochemistry Laboratory at GEOMAR. All methods have been used successfully on sediments from the Okhotsk Sea (cf. Nürnberg et al., 2011; Nürnberg and Tiedemann, 2004). Chlorins were extracted with acetone under sonication and subsequent centrifugation in three consecutive steps; samples were ice-cooled after each extraction. Pigments were acidified with HCl to transform chlorophyll-a into phaeopigments. The sediment extracts weremeasured with a Turner TD-700 fluorometer (GAT) immediately after the third extraction under low light conditions to hinder decomposition. Chlorophyll-a (sigma), acidified with 2 ml HCl was used as standard. To check extractions and instrument drift an internal standard sample was measured after a dozen measurements. Precision of the method is about ±2% and all chlorin concentrations are reported in ng/g (e.g. Fig. S4).

Measurements of biogenic opal concentrations followed the automated leaching method (Müller and Schneider, 1993), in which opal is extracted from the previously freeze-dried, homogenized bulk sediment with NaOH at about 85 °C over c. 45 min. time. The leaching solution is continuously analyzed for dissolved silicon by molybdate-blue spectrophotometry and a mineral correction was applied (DeMaster, 1981). The long-term accuracy of the method is ±0.5 wt %, deduced from replicate and in-house standard measurements (Nürnberg and Tiedemann, 2004).

A CARLO ERBA CNS analyzer (Model NA-1500) was used for measuring the carbon and nitrogen content of sediment core samples (Verardo et al., 1990). The total carbon (TC) content was measured from bulk sediment previously homogenized by milling, the Total Organic Carbon (TOC) content was measured on bulk sediment samples previously decalcified with 0.25 M HCl. The $CaCO_3$ content was calculated by subtracting the TOC from the TC value and using the formula: $CaCO_3 = 8.333 \cdot (TC - TOC)$. Long-term analytical precision is around 2%.

3.5. Chlorophycean freshwater algae

For chlorophycean freshwater algae counts, 32 samples were analyzed for *Pediastrum* spp. and *Botryococcus* cf. *braunii*. Between one and two gram bulk sediment samples were taken in 5–20 cm intervals from core 4 (Kokfelt, 2003). Preparation included (1) 10% HCl treatment to dissolve carbonates, sieving with deionized water through a 6 μm mesh, (2) 40% cold Hydrofluoric Acid and H2O washing, (3) hot 10% KOH treatment to remove humic acids, (4) acetolysis treatment with acetic acid - anhydride mix and concentrated sulphuric acid (9:1) to remove cellulosic matter. Sediment was washed in glacial acetic acid and subsequently rinsed with H_2O. Samples were counted under a Zeiss Axiophot light microscope with phase contrast properties under 400× magnification. Total slides were counted to prevent effects of fractionated grain distribution in the slide, and between 229 and 529 (avg. 437) pollen grains were counted in each sample. For obtaining algae concentrations the freeze-dried sediments were spiked with *Lycopodium clavatum* tablets and calculation followed:

$$C = (X(spike)/X(sample) * k)/m,$$

where X (spike) was the number of *Lycopodium clavatum* spores added to sediment, X (sample) the number of added *Lycopodium clavatum* spores counted, k is the number of the counted palynomorphs in the sample, and m the weight of freeze-dried sediment in gram.

3.6. Bulk elemental XRF scanning

We used XRF scanning to determine bulk sedimentary geochemistry with high resolution. Cores were measured on the CORTEX and AVAATECH XRF scanners in the IODP Bremen Core Repository (Jansen et al., 1998) at 1 cm scanning steps. Details of the setup and analytical protocols of both scanners have been described previously (Richter et al., 2006; Röhl and Abrams, 2000; Tjallingii, 2006; Weltje and Tjallingii, 2008). On the CORTEX system a single run with 10 KV was used for cores 4 and core 79, the AVAATECH scanner was used for core 13 with dual runs on 10 KV and 50 KV. We use data from XRF-scans as qualitative indicators or relative concentrations in the form of count ratios. However, quantification and inter-calibration of XRF relative scanning intensities was obtained by measuring a set of representative discrete sediment core samples taken at count minima and maxima (cf. Weltje and Tjallingii, 2008) from core 4 (Biebow et al., 2002) on an X'Unique XRF spectrometer with Rh tube housed at GEOMAR (D. Rau, per. communication). All reported elements were inspected if they followed a linear regression between discretely sampled and XRF-scanned samples, all showed excellent correlation with R^2 values between 0.97 and 0.91 (Lembke-Jene, 2013).

We apply XRF-scanning-based iron counts normalized to potassium (Fe/K ratios) to qualitatively determine the changing amount of sedimentary iron within the terrigenous sediment fraction. We use potassium instead of other commonly employed elements for normalizing ratios (like Al or Titanium), as it is reliably recorded in both different scanners (the older CORTEX system does not generate Al counts). More importantly, potassium is (1) as well suited as the more often used Aluminium in reflecting background terrigenous sedimentation (cf. Fig. S5 for linear correlation between Al and K in core 13), and (2) least influenced by differential transport processes (Chebykin et al., 2015; Goldberg et al., 2005; Gorbarenko et al., 2002). In comparison to potassium, titanium, an element frequently used for normalization in terrigenous pelagic settings, may not change fundamentally between glacial and interglacial conditions in its abundance, but is influenced by preferential transport processes, in our case sea ice vs. river transport, which we think play fundamental roles in the distribution of the lithogenic fraction on the Sakhalin margin (Chebykin et al., 2015; Yasuda et al., 2014).

4. Results

4.1. Age models

All ages are given in calibrated years before present with reference to 1950 CE as either “cal. yr BP” or “ka”. Ice core record timescales originally referenced to 2000 CE or “b2k” were corrected accordingly. Age models for the three cores are based on AMS ^{14}C dates on planktic foraminifera and in two cases, where abundance of planktic foraminifera was too low to permit dating, on benthic mollusk shells. We used a regional reservoir age correction (ΔR) value of 500 yr ± 50 yr, in line with published correction values for the Okhotsk Sea (Kuzmin et al., 2007) and earlier works (Max et al., 2012; Okazaki et al., 2014). While ΔR values used here potentially changed over the last 18 kyr (Gebhardt et al., 2008; Sarnthein et al., 2007), recent studies in various locations of the North Pacific, the Okhotsk and Bering Sea have provided substantial evidence that variations were of small enough magnitude to justify keeping values constant over the entire age scale reported here (Cook and Keigwin, 2014; Kuehn et al., 2014; Serno et al., 2015). In the lower part of core 4 we used two benthic ages from mollusks. The benthic ^{14}C age in the lowermost part of the core that we took to supplement the benthic-planktic ventilation age differences (Fig. 5b) was

not used in the construction of the age model. We set an additional offset for the ventilation age correction for benthic values of 360 ^{14}C years, based on our own measured benthic-planktic age differences from the same depth interval in nearby core 13 (Table S3) and published data (Max et al., 2014). In the case of core 79 we had to use one additional benthic age control point, this value was corrected by an additional 500 ^{14}C years based on published values for the same time interval from corresponding water depths and nearby cores (Gorbarenko, 2007a, 2010).

We checked potential age-depth relationships by comparing the chlorin records of the cores on their respective independent depth scales against each other, constrained by each cores' individual AMS ^{14}C age tie points (Fig. S4). We assumed that major changes in surface productivity patterns at almost identical locations should be broadly similar in timing to each other within the overall error of the individual age models. In the case of core 13, we were thus able to transfer a set of ^{14}C ages measured in core 79 to core 13, in a mode similar to earlier stratigraphic correlations from this region (Galbraith et al., 2007; Max et al., 2012, 2014). We then used this set of newly transferred ages together with original ^{14}C dates used in an earlier study (Max et al., 2014) to establish a revised age model. For core 4, no correction of the initial independent age model was deemed necessary. We used the program CALIB 6.1.1 and Calib 7.0.1 MARINE 13 calibration curves (Reimer et al., 2009; Stuiver and Reimer, 1993) for initial age determinations (all AMS ^{14}C ages, calibrated age ranges suppl. Table S2).

To establish final age-depth relationships between our age control points we used the routine CLAMS written for the software package R (Blaauw, 2010) as a compromise between manually fitting regressions between age control points and more sophisticated, statistically superior age-depth modeling routines (Blaauw and Andres Christen, 2011; Blaauw et al., 2010; Blockley et al., 2007). The final best-fit runs were performed in CLAMS with 10,000 iterations using a smooth spline function for matching all age control points in their respective 2 σ calibrated age distribution ranges (Fig. 3). Alternative control runs in CLAMS with linear interpolations and higher order polynomial fits displayed only minor offsets within the principal error of the age control points, but the latter yielded higher regression residuals and were thus discarded. Due to the nature of CLAMS and the chosen fitting procedure, the age-depth relationship is based on the entire core and thus reported here; however, in this study we only focus on the deglacial and early Holocene time. In the case of core 13, our new age model differs slightly from the one reported earlier (Max et al., 2014) that encompassed only the deglacial part of the core, as that earlier model was based on linear interpolation between single age control points and less AMS ^{14}C dates available. However, in general, age deviations are less than a few hundred years across the deglacial section discussed here.

According to the age models, average sedimentation rates in the studied time interval (8–18 ka) vary from 15 to 75 cm/ka (southernmost core 4), from 58 to 250 cm/ka (northern deep core 79), and from 88 to 300 cm/ka (northern shallow core 13), thus yielding high, centennial resolution for most proxy series over the deglacial interval.

4.2. Intermediate water ventilation records

Both cores 4 and 79 show significant variations in their epibenthic $\delta^{13}C_{Cib}$ signatures that follow a similar trend, albeit with smaller-scale differences between the two records (Fig. 4). Our southern core 4 records very negative minima of −1.5 and −1.2‰, respectively, during the onsets of the B-A and PB warm phases, whereas its other data fall nearly in line with the records of the northerly core 79 and corresponds to published values $\delta^{13}C_{Cib}$ of the closely related species *C. lobatulus* in core 13 (Max et al., 2014). The observed amplitude of stadial-interstadial $\delta^{13}C_{Cib}$ variations is higher than 0.5‰ for both transitions, significantly exceeding the glacial-interglacial carbon isotope shift of about 0.3‰. As modern values for $\delta^{13}C_{DIC}$ in the OS commonly range between −0.3 and −0.5‰ (Bauch et al., 2002; Itou et al., 2003), we note that deglacial $\delta^{13}C_{Cib}$ values never reached modern values during the glacial termination after observed ventilation maxima during HS-1 (Max et al., 2014; Okazaki et al., 2014), suggesting a deglacial OSIW on average less oxygenated than today, while apparently not reaching the extreme oxygen depletions in other regions (Kuehn et al., 2014). The endobenthic $\delta^{13}C_{Uvi}$ curves of both northerly cores 13 and 79 resemble the epibenthic values in their patterns, though amplitude variations are more pronounced between interstadial low $\delta^{13}C_{Uvi}$ and high $\delta^{13}C_{Uvi}$ data, with average differences of 0.7‰ and more (Fig. 4). Absolute minima are reached during the PB and middle to late Allerød, though this assessment might be biased due to the absence of *Uvigerina* spp. from the benthic species assemblage in the peak Bølling interval, indicating potentially even lower O_2 bottom and pore water concentrations (Bubenshchikova et al., 2008).

The compiled OSIW ventilation (B-P) ages (Fig. 5) help to establish connections between OSIW formation and concurrent deglacial southerly NPIW dynamics, as evidenced in sites from the NE Japanese margin. Both the upper and lower OSIW B-P ages show remarkably little variation of less than 200–300 yr over the deglaciation into the Holocene (Fig. 5b). Absolute B-P ages are comparable to, or generally slightly lower than modern values in the North Pacific (Broecker, 1991). In fact, if error values are included, the OSIW B-P ages remain nearly unchanged between the cold HS-1, warm B-A and the Holocene. In addition, during the Bølling-Allerød warm phase, the internal water mass structure between the upper and lowermost cores stays relatively invariant, indicating no large changes occurred in the physical structure and vertical stratification (Fig. 5).

This is contrasted by NE Japan margin B-P ages that show clear variations in B-P ages in the upper NPIW (Fig. 5a). Values similar to the upper OSIW (about 300–500 yr) during the cold HS-1 are followed by drastic and rapid drops to much lower values of 1200–1400 yr during the B-A and a recovery to better ventilated NPIW waters in the subsequent YD and PB. During both the B-A and the PB the B-P ages on the NE Japan margin appear older than in the Okhotsk Sea at comparable water depths (Fig. 5).

4.3. Productivity variations, lateral terrigenous matter and nutrient supply

Both total organic carbon (TOC) and chlorin concentrations follow a pattern evident in all cores, with maxima during the mid-late Allerød and peak values during the PB, especially in the more northerly cores 13 and 79 (Fig. 6). Deep Core 79 records maximal chlorin values during the PB and the highest amplitude variations. Notably, southern core 4 does not record a distinct productivity peak in chlorin during the B-A, in contrast to northern cores and other sites further downstream. $CaCO_3$ concentrations in cores 4 and 79 (Fig. 7) follow the pattern recorded in the other bulk productivity proxies (Fig. 6), while biogenic opal concentrations show a late increase from uniformly low values of about 5% to steadily increasing early Holocene maxima of about 25% (Fig. 7). In particular, opal concentrations do not exhibit the rapid millennial-scale variations expressed in all other biological productivity proxies.

The studied interval is characterized by rapid changes in C/N ratios in cores 4 and 79. Elevated C/N ratios are recorded in both cores during the warm interstadial B/A and PB periods of the termination, with maxima in both cores during the PB phase and

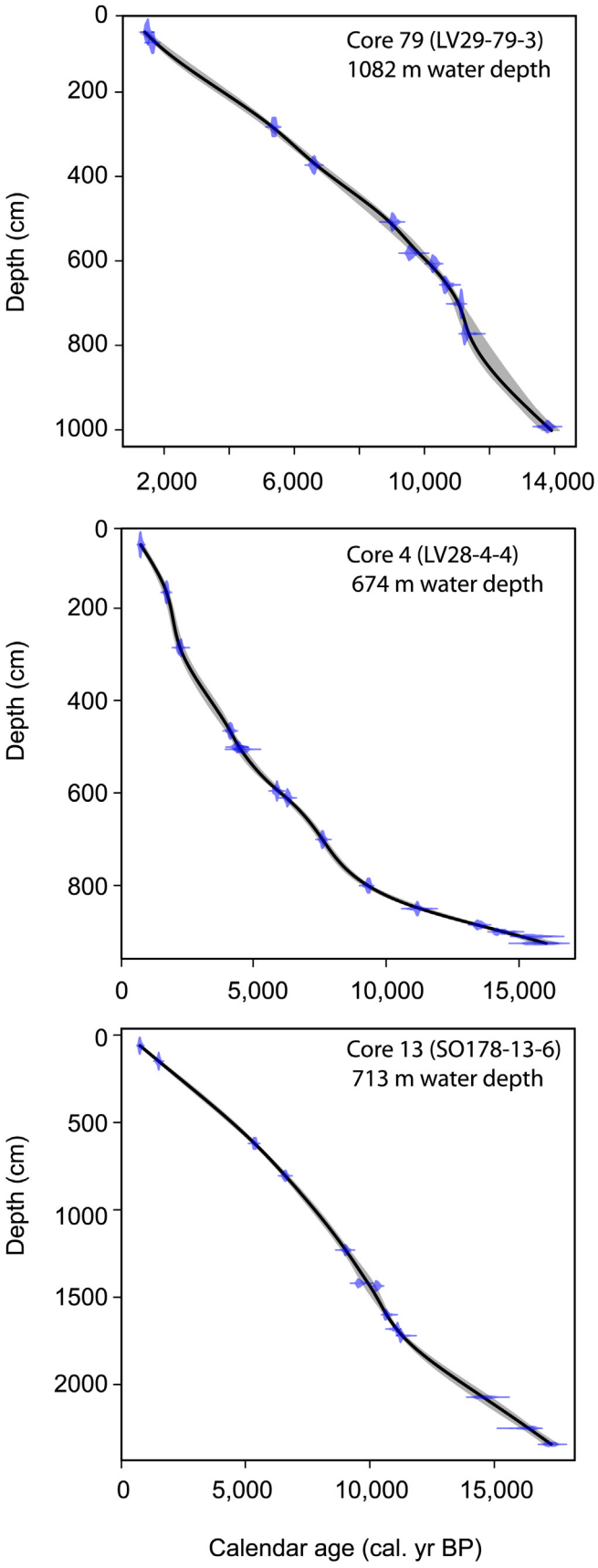

Fig. 3. Age models for cores used in this study. Age-depth relationships derived for individual cores from CLAMS runs. Blue markers show calibrated AMS ^{14}C ages (in cal. yr BP) against core depths (in cm) with 2σ error range distributions, Black line are ideal least squares error fit, grey shaded areas show calculated 2σ uncertainty ranges of the smooth spline fit models. Upper panel: Core LV29-79-3, middle panel: Core LV28-4-4, lower panel: core SO178-13-6, modified from initial age model published in Max et al. (2014) by additional age control points transferred from LV29-79-3. (For interpretation of the references to colour in this figure legend, the reader is referred to the web version of this article.)

early Holocene (Fig. 8). Northern core 79 shows higher, maximum values of 11–14 in the late PB, with a second, albeit smaller peak of about 11 in the late Allerød, indicating a major influence of lateral transport of terrigenous particulate organic carbon (POC) to the core site. Southern core 4 shows a general pattern of elevated C/N ratios during inceptions of the warm Bølling and PB phases, however, the overall amplitude of the signal appears more muted with values reaching maxima of only 9–9.5, significantly lower than in core 79 and in line with a more distal location to the northern source areas for terrigenous POC (Fig. 7e). However, we note that the TOC concentration and C/N ratios are not linearly correlated in either of the two cores.

XRF-derived Fe/K ratios indicate an increase in Fe delivery to the core sites during interstadial warm phases, with an overall increasing trend towards the Holocene (Fig. 8 d–e and 11d). The observed increases are interrupted by minimal values during the cold HS-1 and YD stadials, whereas local maxima occur during the Allerød and the late PB around 10.2 ka. The differing ratios we report are due to the fact that we, unfortunately, had to use two different XRF scanner types for the study, an older CORTEX Scanner for the cores 79 and 4, and an Aavatech XRF scanner for core 13. The sedimentation rates are more similar between cores 79 and 13, with core 4 having a lower sedimentation rate during the deglacial, due to its more distal location to the main sediment source areas (river discharge, sea ice transport), explaining the very slightly higher count ratios in core 79 (Fig. e) than in core 4 (Fig. 4f), which were both measured on the same scanner. Our sedimentary Fe/K ratios are assumed to reflect delivery of Fe to the core sites by the turbid OSIW and DSW, respectively, that passes directly over our sites. Its origin was tracked to the northern shelf areas and the Amur river discharge, where Fe is entrained both from surface sediments by tidal currents and surface river runoff during intense mixing processes on the shallow northern shelf areas into DSW/OSIW (Nakatsuka et al., 2004a; Nishioka et al., 2014b; Nishioka et al., 2007). A number of recent studies based on sediment traps, water column measurements as well as sediment surface sample data have consistently shown that the concentrations and processes of Fe deposited along the Sakhalin margin are directly related to upstream entrainment dynamics into intermediate-depth concentration maxima both in dissolved and particulate iron (Fe) in OSIW that is ultimately transported into the North Pacific (Nakatsuka et al., 2004a, 2009; Nishioka et al., 2014b, 2007, 2011; Uchimoto et al., 2014).

Low-resolution freshwater algae counts from our southernmost core 4 location indicate that a first, smaller discharge occurred during the B/A with Pediastrum spp. concentrations reaching 2335 spec/g, followed by a higher freshwater discharge event between 11 and 9 ka, where concentrations in two samples peaked at 21,380 and 12,700 spec./g sediment, respectively (Fig. 9a and b). Freshwater algae concentrations during these two peaks are more than an order of magnitude higher than most Holocene and modern values, with uppermost samples in core 4 yielding concentrations of 51–149 spec./g sediment over the last 1 ka, confirming that neither *Pediastrum* nor *Botryococcus* taxa occur in substantial numbers at site 4 today (Fig. 9b). As a result of long-range transport from the Amur river, green algae are often viewed as pure freshwater forms, but *Pediastrum* species are also known to occur in

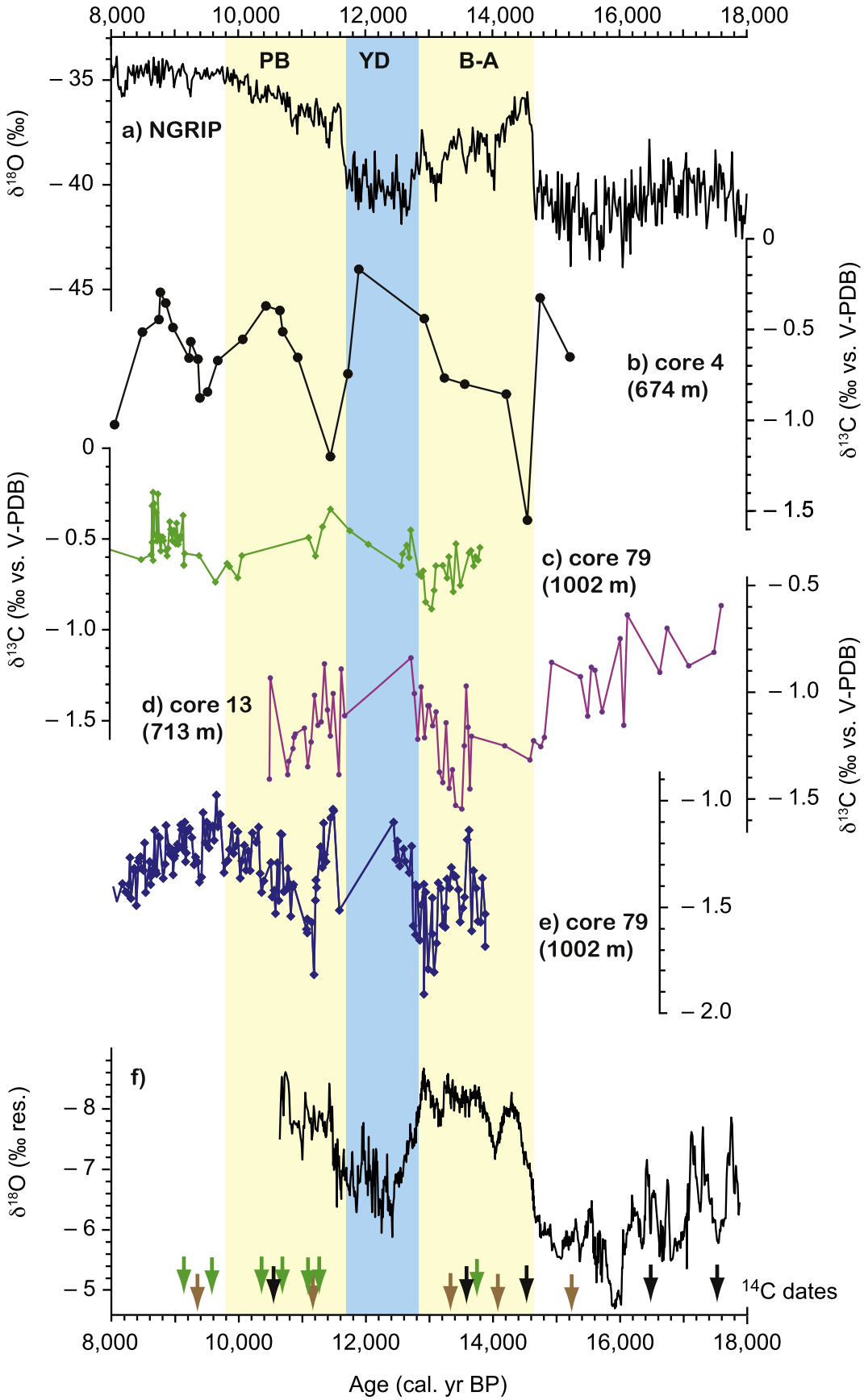

Fig. 4. Proxy time series for OSIW oxygenation, with Northern Hemisphere reference records from high (Greenland) and low (China) latitudes. (a) Greenland NGRIP $\delta^{18}O$ on the timescale of Rasmussen et al. (2008); (b) *C. mundulus* $\delta^{13}C_{cib}$ from southern shallow core 4 (black), (c) *C. mundulus* $\delta^{13}C_{cib}$ from northern deep core 79 (green); (d) *U. peregrina* ($\delta^{13}C_{Uvi}$) from northern shallow core 13 (violet), (e) from northern deep core 79 (blue); (e) $\delta^{18}O$ time series of Hulu Cave speleothem record (Wang et al., 2008) on timescale of Southon et al. (2012). Yellow shadings: warm interstadial phases B/A and PB, blue shading cold stadial YD phase. Arrows on bottom: AMS ^{14}C dates used in age models, colors indicate core 13 (black), core 79 (green) and core 4 (brown). (For interpretation of the references to colour in this figure legend, the reader is referred to the web version of this article.)

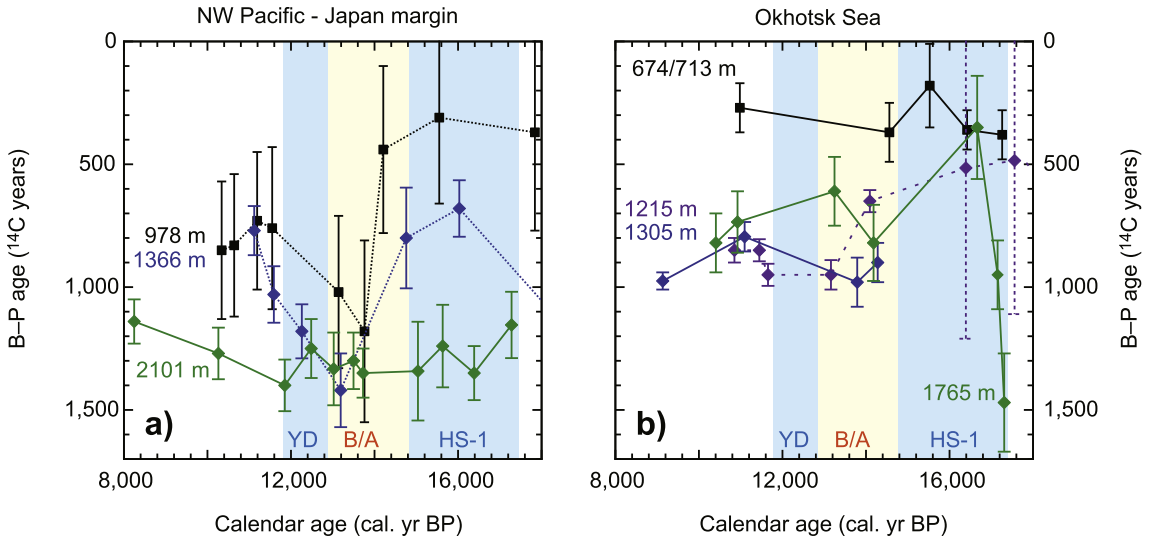

Fig. 5. Compilation of Benthic – Planktic ventilation ages based on published and this study. (a) Data from the NE Japan Margin off Shimokita. Three cores from shallow (CH84, black, Duplessy et al., 1989), intermediate (blue, Ahagon et al., 2003; Ahagon and Uchida, 2004; Ohkushi, 2004), and deeper (green) water masses (green, Okazaki et al., 2012). (b) Data from the Okhotsk Sea margin cores influenced by the WSAP waters and OSIW fromation. Black: shallow core 4 (this study),: intermediate cores MR06-04 PC04A/B (violet) (Okazaki et al., 2014) and LV27-2/4 (Gorbarenko et al., 2010; Gorbarenko et al., 2007), and deeper core LV29-114-3 (Max et al., 2014). Blue shading marks Heinrich Stadial 1 and Younger Dryas cold intervals, yellow shading the warm Bolling-Allerød intervals. (For interpretation of the references to colour in this figure legend, the reader is referred to the web version of this article.)

brackish environments with salinities higher than 10 psμ (Matthiessen and Brenner, 1996). Previous work on surface sediments in the Arctic Ocean has shown that the concentration of the algae *Pediastrum* spp. decreases with the distance from the river mouth, whereas *Botryococcus* spp. in general is more evenly distributed into outer shelf and deep sea sediments (Matthiessen et al., 2000). This behavior is partly caused by a high buoyancy, but also *Botryococcus* spp. colonies tolerate higher salinities than *Pediastrum* spp. and are likely to survive longer in the brackish conditions of a freshwater plume.

5. Discussion

5.1. Collapsed OSIW formation vs. oxygenation minima during deglacial warm phases

Two principal, non-exclusive mechanisms could account for the observed interstadial (B-A and PB, Fig. 4b) ventilation minima of the OSIW layer. Either formation of DSW and thus well-ventilated OSIW ceased due to physical forcing and circulation pattern different from today, leading to little to no export of OSIW from the Okhotsk Sea into the open North Pacific. Such a collapse of OSIW production would be caused by an absence of seasonal sea ice, and thus polynia-induced brine rejection, leading to DSW formation. Alternatively, OSIW was still produced (potentially with less vigorous entrainment of O_2) and exported out of the Okhotsk Sea similarly to modern conditions, but its initial oxygen content was lower due to shortened atmosphere-ocean exchange and more intense organic matter remineralization after formation because of higher nutrient loads. In the latter case, it likely faced increased POC and DOC consumption and respiration already on the Sakhalin margin soon after formation, rapidly decreasing the already lower-oxygenated OSIW even further.

We favor the second explanation as more important factor for the following reasons: Previous works have shown, based on IRD provenance and abundance studies, that sea ice was present during all phases of the deglaciation in the northeastern part of the Okhotsk Sea and on the Sakhalin margin, even if overall abundances increased and decreased with cold and warm phases (Gorbarenko et al., 2004, 2010; Nürnberg et al., 2011; Sakamoto et al., 2005). We thus presume that necessary physical preconditions for sustained formation of DSW masses were fulfilled, i.e. opening of polynias and formation of brine rejections during cooling in winter. However, the maximum duration of the sea-ice season and thus the intensity of atmosphere-ocean exchange and DSW ventilation in winter polynias were likely shortened due to the stronger seasonality and stronger deglacial freshwater flux into the Okhotsk Sea via the Amur. The latter inhibits sea ice growth in winter seasons due to the high amounts of sensible heat it carries in its late summer discharge peaks from lower latitude monsoon-influenced regions (Ogi et al., 2001; Tachibana et al., 2008). Still, some ventilation and O_2 entrainment into OSIW likely persisted even in warm deglacial phases, supported by the notion that despite high productivity, the occurrence of prominent laminated intervals in the mid-depth Okhotsk Sea is not observed in the cores 13 or 4, like at nearly all other mid-depth North Pacific locations where they indicate transient anoxia during the B/A and PB warm interstadials (Jaccard and Galbraith, 2011; Kuehn et al., 2014).

In addition, our $\delta^{13}C_{Cib}$ data reported here and earlier (Max et al., 2014) indicate that the vertical extension of OSIW between our shallower and the deeper sites remained surprisingly homogenous over stadial-interstadial transitions. We thus presume that if a substantial weakening of OSIW formation rate or flow volume during warm interstadial phases had happened, an increasing $\delta^{13}C_{Cib}$ gradient between deeper core 79 (1002 m) and shallower cores 4 and 13 (673/713 m) should have appeared, because core 79 is at the deepest potential extension of intermediate depth water and more sensitive to switches between better ventilated OSIW and deeper, oxygen-poorer PDW. However, no such dynamic change can be observed. To the contrary, during shorter intervals in the warm B/A around c. 13.4–13.8 ka, and in the PB around c. 9.4–10.8 ka and 10.8–11.8 ka, we observe lower $\delta^{13}C_{Cib}$ values in upper core 4 compared to lower core 79 (Fig. 4b and c). Such a pattern is not easily explainable by mixing between deeper, low-$\delta^{13}C$ PDW and shallower mid-depth, high $\delta^{13}C$ OSIW end members alone, pointing instead to additional processes that influence the $\delta^{13}C$ signal and

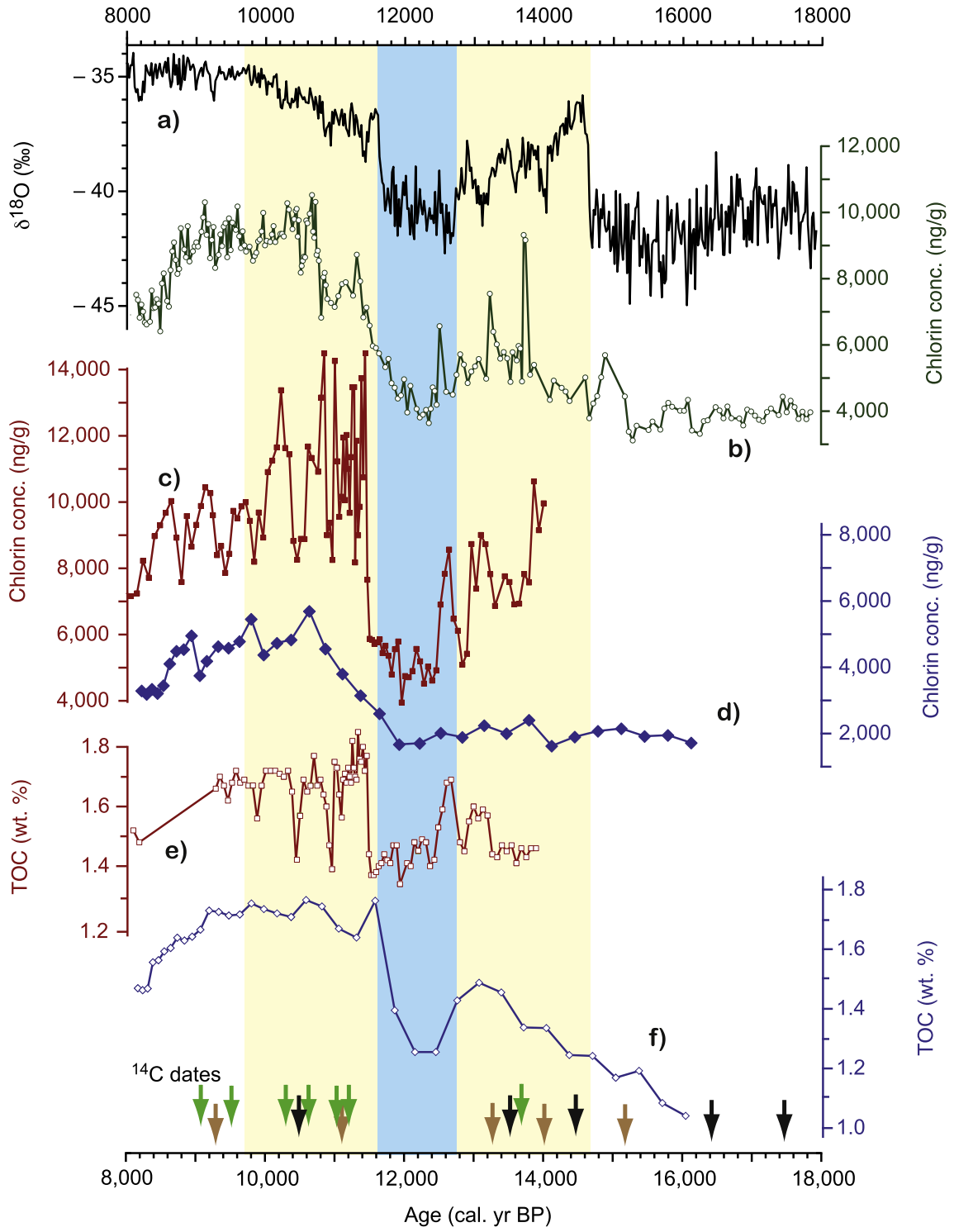

Fig. 6. Bulk productivity proxies. (a) Greenland NGRIP $\delta^{18}O$ on timescale of Rasmussen et al. (2008); chlorin concentration from this study's cores in (ng/g) from: (b) northern shallow core 13 (dark green, empty circles); (c) northern deep core 79 (dark red, filled circles); and (d) southern shallow core 4 (blue, filled diamonds). Concentrations of total organic carbon (TOC) of this study's cores from (e) northern deep core 79 (dark red as in (c), but empty squares); (f) southern shallow core 4 (dark blue, empty diamonds). Rest as Fig. 4. (For interpretation of the references to colour in this figure legend, the reader is referred to the web version of this article.)

thus core layer OSIW ventilation.

Indeed, we recorded co-variations of epifaunal $\delta^{13}C_{Cib}$ and shallow infaunal $\delta^{13}C_{Uvi}$ data (Fig. 4b–e), which indicate that the $\delta^{13}C_{DIC}$ and also O_2 concentrations of OSIW were to some extent determined by mesopelagic respiration. As such remineralization processes are most active within the core layer of the high-OM turbid OSIW core layer, i.e. in the 400–1000 m water depth range, the oxygenation of OSIW was likely significantly reduced already close to the formation region during deglacial warm phases, corroborating earlier hypotheses based on export production records from the pelagic North Pacific (Crusius et al., 2004). In analogy to modern observations, a minimum of about 30% of the

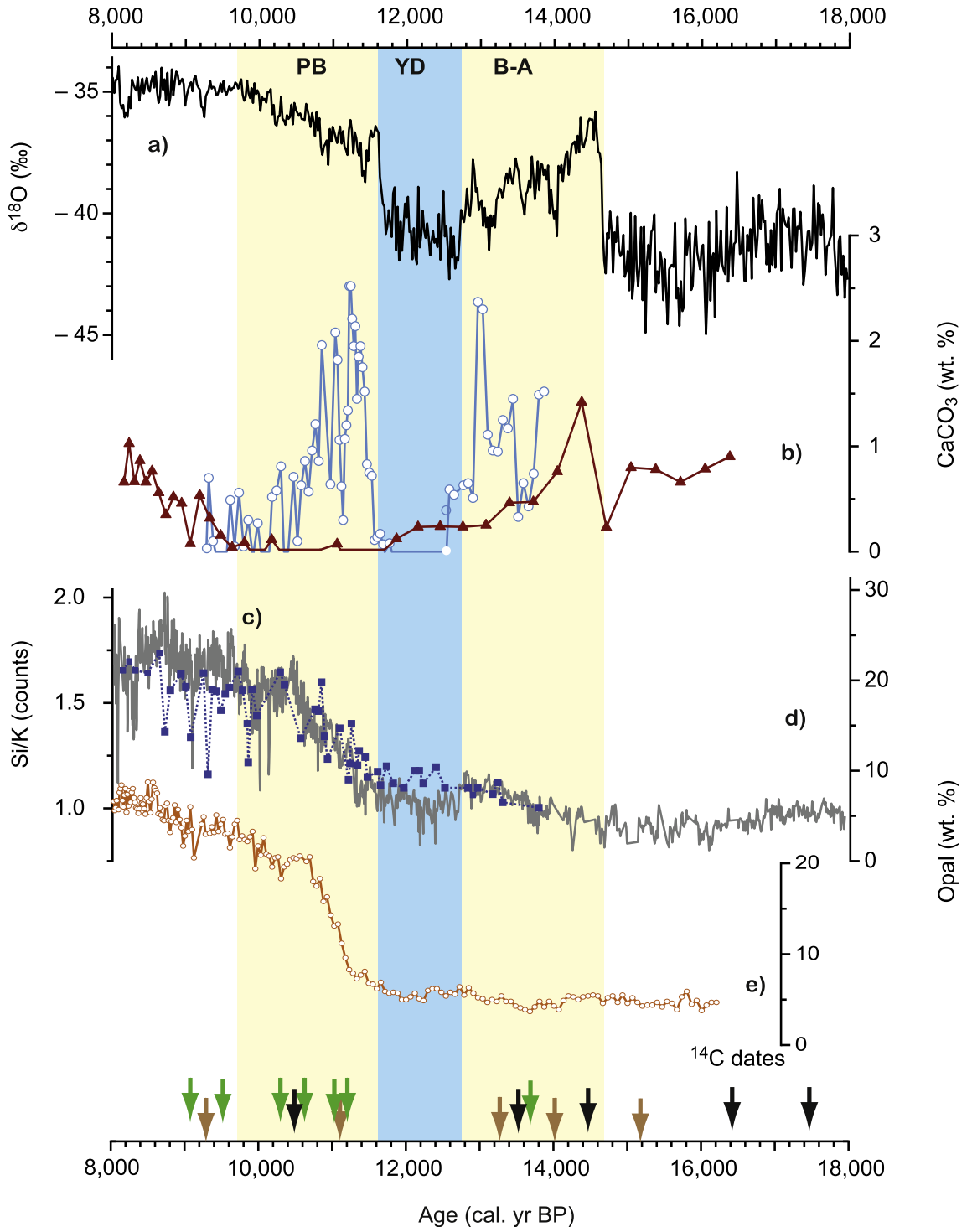

Fig. 7. Carbonate and siliceous productivity and terrigenous proxy time series. (a) Greenland NGRIP $\delta^{18}O$ on the timescale of Rasmussen et al. (2008). $CaCO_3$ concentrations from this study's cores (all in weight %) from: (b) northern deep core 79 (light blue, empty circles) and southern shallow core 4 (brown, filled triangles); (c) biogenic opal of northern deep core 79 (blue, filled squares), together with closely matching XRF-derived Si/K ratios as proxy for opal concentrations of nearby shallow northern core 13 (black line). (e) Concentrations of biogenic opal (weight %) of southern shallow core 4. (f) $[C/N]_{atomic}$ ratios of southern shallow core 4 (dark red, empty circles) and northern deep core 79 (dark blue, filled diamonds). (For interpretation of the references to colour in this figure legend, the reader is referred to the web version of this article.)

mesopelagic waters' initial O_2 concentration was likely consumed relatively quickly by organic matter respiration (del Giorgio and Duarte, 2002; Herguera et al., 2009).

The Benthic–Planktic (B-P) ventilation ages derived from our and other cores (Gorbarenko et al., 2007, 2008) in the Okhotsk Sea from water depths of 675 m (OSIW core layer) and 1300 m (lower OSIW) support our hypothesis, because they show no major coherent changes towards previously proposed simply higher B-P ages during the B-A and PB. We observe that while increases in NPIW ventilation and formation did occur during the cold stadial phases (HS-1 and YD) in the North Pacific (Okazaki et al., 2010), the warm interstadial phases in contrast did not result in persistent

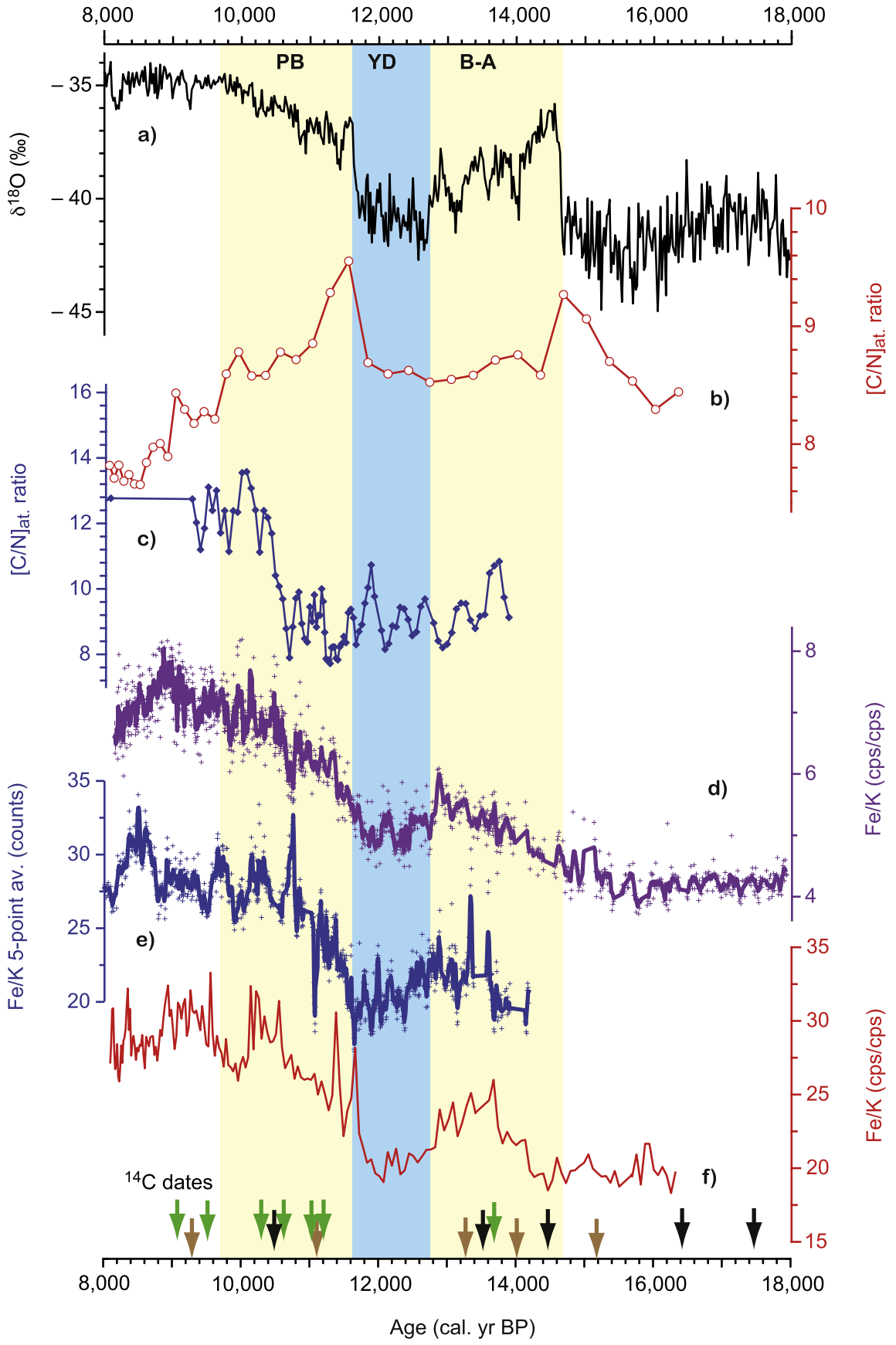

Fig. 8. Comparison of proxy time-series indicative of terrigenous sediment transport. (a) Greenland NGRIP $\delta^{18}O$ on the timescale of Rasmussen et al. (2008). (b) $[C/N]_{atomic}$ ratios of southern shallow core 4 (dark red, empty circles) and (c) northern deep core 79 (dark blue, filled diamonds). (d–f) XRF-scanning-derived Fe/K ratios for all cores in this study. (d) Fe/K ratio of northern shallow core 13 (violet line 5 point running average, violet crosses individual values). (e) Fe/K ratio of northern deep core 79 (blue line 5 point running average, blue crosses individual values). (f) Fe/K ratio of southern core 4 (red line). Remainder as in Fig. 4. (For interpretation of the references to colour in this figure legend, the reader is referred to the web version of this article.)

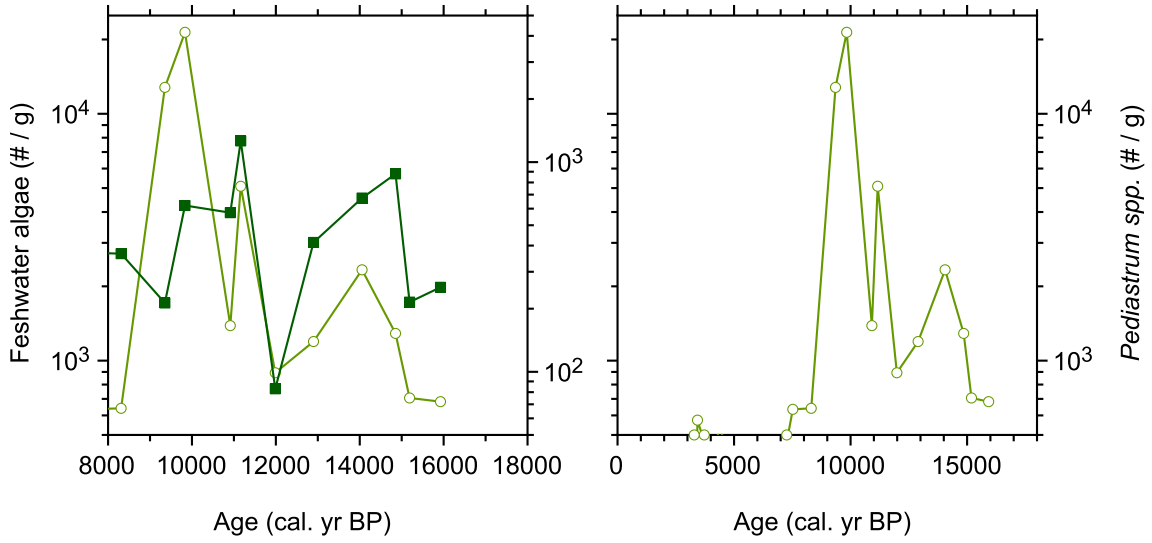

Fig. 9. Concentrations (in numbers/g sediment) of freshwater-restricted chlorophycean algae *Pediastrum* spp. (light green, open circles) and freshwater-brackish-restricted *Botryococcus* spp. (dark green, filled squares), counted in core 4 and used as proxies for fluvial freshwater supply to eastern Sakhalin continental margin. Note logarithmic scale for concentrations. (Left) Interval studied from 8 to 18 ka. (Right) entire core section on scale 0 to 18 ka. Note that nearly no freshwater algae are found at this location under modern (still large) fluvial discharge conditions from Amur, implying substantially larger discharge during the deglacial interval. (For interpretation of the references to colour in this figure legend, the reader is referred to the web version of this article.)

older water masses compared to the modern situation in the OSIW source region, implying a mode similar in strength and volume to modern circulation patterns or even stronger. This reasoning is in line with the notion that the global Meridional Overturning Circulation as one forcing for variations in North Pacific circulation was comparable to modern conditions (McManus et al., 2004) or stronger as evidenced in records from the Atlantic region during the B/A (Barker et al., 2010).

However, a collapse of NPIW ventilation off Japan between 900 and 1400 m is indicated by the drop of B-P ages to much older values characteristic of deeper PDW values around 2100 m water depth (Fig. 5a). This pattern implies that either upwelling of old, deeper water masses occurred at the Japan margin into intermediate depths without reaching the surface ocean, or that circulation patterns in the intermediate water layer off Japan significantly changed to old water masses during the B/A (Okazaki et al., 2014), while leaving deeper PDW around 2000 m relatively unaffected at the same time (Okazaki et al., 2012). Some works indicate that the boundary between Kuroshio and Oyashio currents shifted by several degrees in concert with stadial and interstadial variations during the last glacial and the last termination (Inagaki et al., 2009; Yamamoto et al., 2005), probably affecting the mid-depth waters at the northern Japan margin sites, switching them between a more northern and southern-derived source. As paleo-ventilation ages in the Okhotsk Sea and by inference the WSAP gyre region (Fig. 5b), i.e. northward of the Kuroshio-Oyashio extension, are apparently unaffected by these changes and show no coherent signature, but only minor variations over the glacial termination, we presume that during transient warm interstadial phases southern subtropically-influenced intermediate water became more isolated from the northern OSIW-influenced WSAP gyre than today. This reasoning is in line with previous evidence from a well-dated mid-depth core in the WSAP-influenced Bering Sea (Kuehn et al., 2014) and indicates an increased injection of more (interstadial low-O_2) OSIW into the northerly subarctic gyre circulation that may have more effectively decoupled deglacial subarctic and subtropical mid-depth water masses in the mid-latitude North Pacific than today. In contrast, during the remainder of the deglaciation, similar B-P ages on the Okhotsk and Japanese continental margins argue for a southward propagation of OSIW-influenced (stadial high-O_2) intermediate waters into lower latitudes, analog to modern conditions. In any case, our compilation outlines a more complex pattern of deglacial North Pacific circulation changes in both large gyre regions than previously assumed (Max et al., 2014; Cook and Keigwin, 2014) and should warrant more detailed study with both proxy reconstructions and modeling.

5.2. Timing and causes for productivity and OSIW ventilation changes during the deglaciation: hinterland environmental changes and forcing

The deglacial O_2 decline during the warm B-A indicated in our $\delta^{13}C_{cib}$ data is accompanied by pronounced maxima in surface ocean productivity (Figs. 4, 6 and 7). However, in contrast to neighboring regions and more southern lower-resolution sites our results place the maxima in primary productivity to the PB (11.6–9 ka) and the Allerød (13.8–13.0 ka), rather than the Bølling or entire B-A phases (Crusius et al., 2004; Gorbarenko et al., 2002; Khim and Sakamoto, 2012). This timing is not strictly correlated to the rapid warming and MOC changes known from the Atlantic (McManus et al., 2004; Piotrowski et al., 2004). Instead, a first small productivity peak occurs slightly earlier around ca. 15 ka, followed by a second stronger peak centered towards the late Bølling to early Allerød (11.6–11.2 ka, Figs. 6 and 7). This timing is corroborated by multi-proxy and benthic species assemblage observations from nearby sites (Bubenshchikova et al., 2010; Gorbarenko, 2007a, Gorbarenko et al., 2010; Seki et al., 2004). There, relatively late increases in mainly carbonate-bearing primary producers, occurring only after the Bølling around 13.6–13.1 ka, were tentatively ascribed to a potential lagged transfer of climatic forcing from the North Atlantic region and changes in the AMOC to the North Pacific, but the timing and causation could not be further verified due to potential age model uncertainties in the investigated core (Gorbarenko et al., 2010). Our new, high-resolution set of cores confirms this particular delayed occurrence (Figs. 6c and 7b) in the Okhotsk Sea.

In other circum-Pacific regions, sudden deglacial spikes in productivity have been ascribed to various causes, like eustatic sea

level rise, mixed layer stratification, lateral material transport or circulation changes (e.g. Addison et al., 2012; Caissie et al., 2010; Cook et al., 2005; Davies et al., 2011). With regard to the effect of these potential causes in the Okhotsk Sea, we assume that flooding of the extensive northern shallow shelf areas during the early deglaciation (18–15 ka) and the pronounced MWP Ia likely enhanced southward transport of lithogenic terrestrial material with the East Sakhalin Current. It has been shown that such shelf-derived supply of additional refractory nutrients supports primary production further offshore (Davies et al., 2011; Klinkhammer et al., 2009). In the Okhotsk Sea, the first pre-Bølling (15 ka, Figs. 6 and 10a-e) and Allerød (13.4–13.0 k) productivity peaks were likely supported by such a mechanism. However, fertilization of marine productivity by se-level alone rise was likely not the main cause for productivity peaks in the Okhotsk Sea due to the following considerations: Absolute deglacial productivity maxima peak later than maximum sea level changes at all sites, namely during the PB with initial spikes around 11.6 to 11.2 ka (Fig. 6b–e, 10b). Thus, reported productivity maxima would be offset in timing and lag the sea-level rise maxima by several thousand years. In addition, hypothetically mobilized terrigenous organic matter was highly refractory and, at least during the early phase of the deglaciation, inundated shelf areas were presumably still frozen and thus relatively inert to sediment mobilization, due to their location within the glacial permafrost region (Chlachula, 2003; Vaks et al., 2013).

For an explanation of these discrepancies, we consulted speleothem and loess records from the low-latitude hinterland region (Fig. 10g–i), which are indicators for the East Asian Summer Monsoon (EASM) temperature (Fig. 10g, Dykoski et al., 2005; Wang et al., 2005) and/or precipitation history (Fig. 10g–i, Peterse et al., 2011). The Dongge Cave speleothem record correlates well in overall shape and pattern with our proxy reconstructions of OSIW ventilation and export production (Fig. 10b–c and e), but diverges in the fine structure. Remarkably, the loess-derived precipitation reconstruction shows that the deglacial EASM increases in precipitation were more gradual than the speleothem $\delta^{18}O$ series suggests (Fig. 10g–i) and thus started later than the initial rapid onset of the EASM temperature increases (Peterse et al., 2011). To establish a link between these hinterland reference records indicative of hinterland climatology and the Okhotsk Sea freshwater influx, we turned to our freshwater algae counts (Fig. 9a and b, 10d) from the southernmost core location (core 4). Results showed the first, smaller discharge peak during the B/A was followed by a larger Preboreal freshwater discharge event. Thus, freshwater algae concentrations during these two peak periods are significantly higher than modern values (Fig. 9b), though modern Amur river discharge and fluvial sediment load is quite substantial (Seki et al., 2014; Yasuda et al., 2014). Even if changes in sedimentation rates and thus overall accumulation may have played a role in changing the concentrations throughout the last 18 ka, we tentatively infer that precipitation increases during the B/A and PB warm phases caused sustained fluvial discharge peaks into the Okhotsk Sea via the Amur. Land-based records from NE-China peat bogs support this scenario, indicating maxima in effective precipitation in the Amur catchment area (Bazarova et al., 2008; Seki et al., 2009a).

Concurrent maxima in terrigenous nutrient and detrital iron load derived from the Amur started in the deglacial between 14 and 12 ka and peaked during the PB as evidenced by maxima in Fe/K ratios (Fig. 8d–f and 10c and e) and matching peaks of terrestrial biomarkers in nearby marine cores (Fig. 10f) (Seki et al., 2003, 2012). These higher-than-modern peaks in terrigenous sediment load were in all probability buttressed by melting of permafrost in the Amur hinterland during the late deglaciation. Though temporally poorly constrained, the melting was mostly dated in terrestrial records to the Preboreal (Bazarova et al., 2008; Sakaguchi, 1992). Hinterland records and nearby organic terrestrial biomarker data (Seki et al., 2012), combine with our sedimentological and freshwater algae data (Figs. 9 and 10) to provide evidence that high amounts of fresh organic matter, nutrients and sediment suspension were supplied to the upper water column of the NW Okhotsk Sea during the warm B-A and PB phases (Figs. 8 and 10). These elevated nutrient were optimally provided to the photic zone, as indicated by maxima in mixed layer stratification (Riethdorf et al., 2013) and longer sea ice-free summer seasons during the deglacial warm B-A and PB (Gorbarenko, 2007a, 2012), thereby supporting primary production increases. This conditioning of the upper mixed layer is also assumed to have provided carbonate producers (coccolithophores) with a competitive advantage over diatoms over the deglaciation, thus explaining the lack of an early deglacial bio-siliceous productivity peak that was reported in a number of previous studies and thus is a coherent feature throughout the Okhotsk Sea (Harada et al., 2008; Khim and Sakamoto, 2012; Okazaki et al., 2014; Seki et al., 2009b).

Together, our data (Fig. 10) indicate that freshwater supply by the Amur was a particularly important factor in rapidly (i.e. within 10–100s of years) supplying relatively fresh terrigenous matter and nutrients for maximum primary production to the Okhotsk Sea continental margin during the B-A and PB warm phases, while sea level rise was likely another important contributor of elevated terrigenous refractory organic matter content. Our results also support a scenario with environmental forcing that is regionalized and differing between particular NW-Pacific areas, being less strictly correlated simply to North Atlantic millennial-scale climatic variability as shown in Greenland ice core records and AMOC changes (Gorbarenko et al., 2008; Harada et al., 2008; Ohkushi et al., 2003; Okazaki et al., 2014). Apparently, in the Okhotsk Sea, low-latitude forcing by hinterland changes through the migration of the East Asian Summer Monsoon front and deglacial changes in the terrestrial cryosphere played an additional critical role in shaping the deglacial hydrography and biogeochemistry.

5.3. Consequences of OSIW biogeochemical variations for deglacial North Pacific productivity pulses and OMZ development

Our results provide evidence for significantly higher organic matter and nutrient loads within the OSIW core layer during the warm interstadial phases of the last glacial termination (Figs. 8, 9 and 11c-d). Based on a number of modern sediment trap and time series results, locations on the Sakhalin margin reliably record the amount of terrigenous and biogenic material entrained in the DSW formation region, which is then transported within a highly turbid OSIW water layer southward into the North Pacific (Hansell, 2002; Nakatsuka et al., 2002, 2004a; Nishioka et al., 2007). Today, the amount of laterally transported POC (0.9 Tg C/yr) and DOC (13.6 Tg C/yr) entrained within DSW/OSIW is considerably larger than the amount of POC that settles through the water column from surface biogenic productivity (0.2–0.5 Tg C/yr; Nakatsuka et al., 2004b). Thus, lateral entrainment and subsequent transport of suspended material, rather than vertical settling of nutrients, preconditions the biogeochemistry of OSIW. Our multi-proxy data imply that the flux of the entrained POC and DOC and terrigenous lithogenic material was even higher than today during the B-A and PB warm phases.

We thus hypothesize that significant amounts of dissolved and particulate terrigenous carbon, as well as nutrients such as $Si(OH)_4$, were laterally transported within the OSIW during the B-A and PB, and exported from the Okhotsk Sea to the pelagic WSAP (Fig. 1, 11). While the modern $Si(OH)_4$ concentrations in the mid-depth water column of the Okhotsk Sea are already relatively high (cf. Biebow and Hütten, 1999), a decrease in deep (PDW) to intermediate-

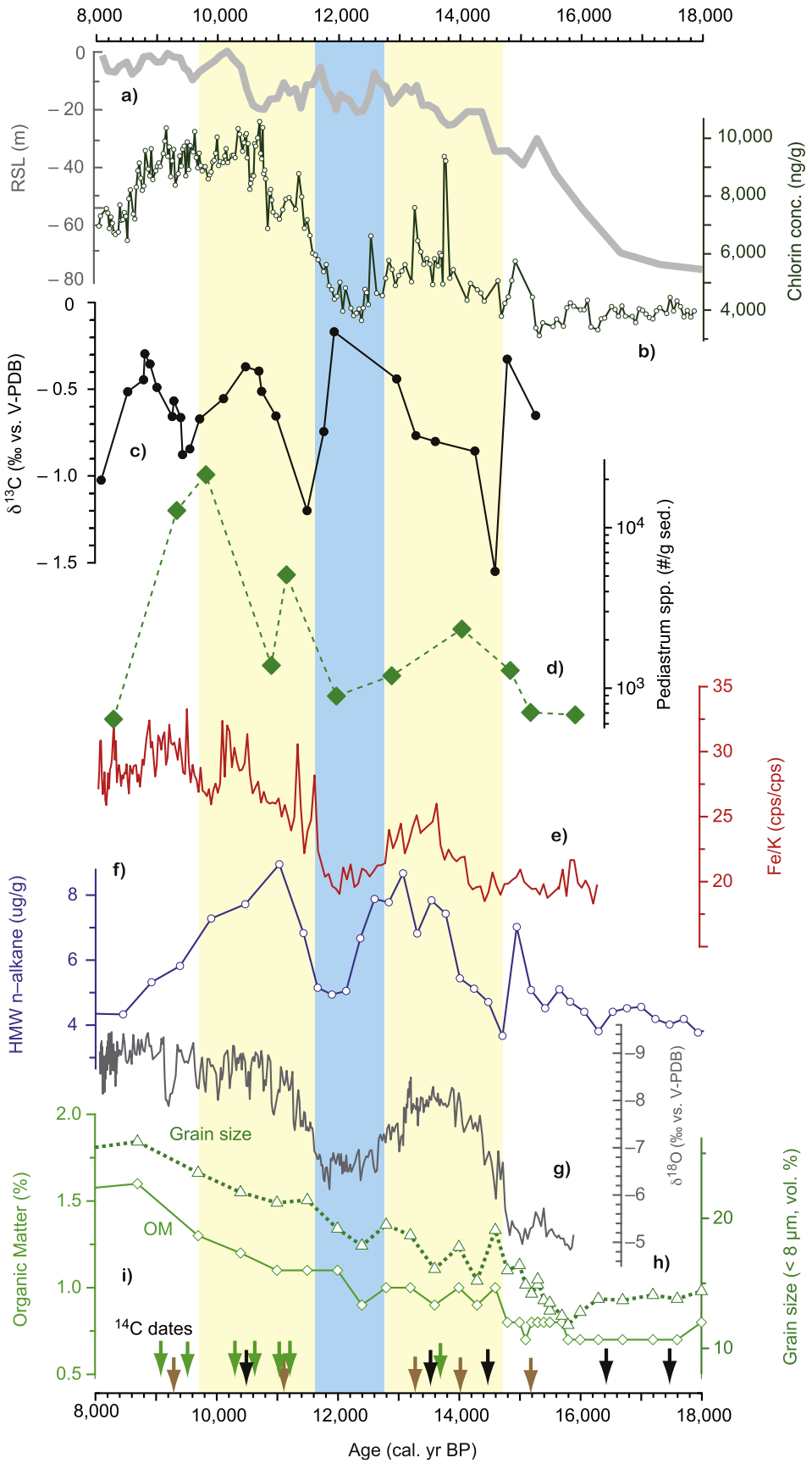

Fig. 10. Synoptic comparison of Okhotsk Sea productivity, terrigenous Fe supply and OSIW changes and Asian hinterland records: (a) eustatic sea level curve (Rohling et al., 2009); (b) chlorin concentration (ng/g) from core 13 (dark green, empty circles). (c) OSIW ventilation record based on epibenthic *C. mundulus* $\delta^{13}C$ from southern shallow core 4 (black). (d) Concentrations (in numbers/g sediment) of freshwater algae *Pediastrum* spp. (green, filled diamonds) in core 4 and as proxy for fluvial freshwater supply to eastern Sakhalin continental margin. (e) XRF scanning-derived Fe/K ratios in core 4 as indicator for riverine/shelf-derived input of micronutrients into OSIW. (f) Terrestrial plant wax biomarker concentrations C_{25}-C_{35} n-alkanes (µg/g) in nearby core C9, indicating shelf submergence and freshwater runoff (Seki et al., 2012). (g) Proxy record for EASM strength and temperature/precipitation changes: Dongge Cave speleothem $\delta^{18}O$ (in ‰ vs. V-PDB, Dykoski et al., 2005). (h) and (h) Proxy records for precipitation in the SE Asian low latitudes as expressed in Mangshan Loess Plateau sequence MS2008E (Peterse et al., 2011); (h) MS2008E grain size distribution as fraction < 8 µm (in vol. %) and (i) organic matter (OM) content (weight %). Rest as in Fig. 4. (For interpretation of the references to colour in this figure legend, the reader is referred to the web version of this article.)

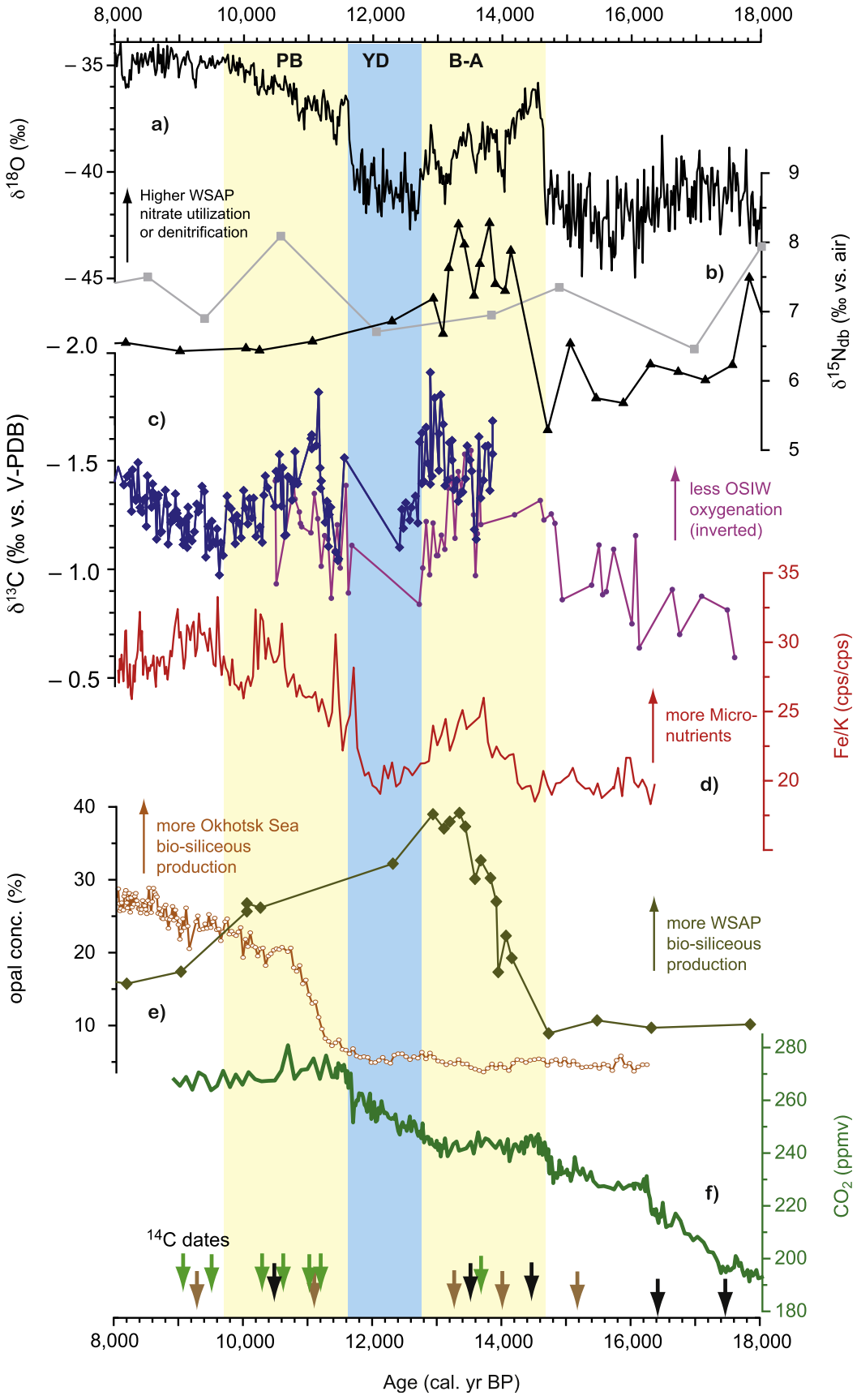

Fig. 11. Synoptic comparison of selected Okhotsk Sea records with downstream pelagic subarctic North Pacific (core PC1, Brunelle et al., 2010) changes in productivity and nutrient utilization to assess consequences of OSIW variability. (a) Greenland NGRIP $\delta^{18}O$ (Rasmussen et al., 2008). (b) nutrient utilization based on diatom-bound $\delta^{15}N$ records for the Okhotsk Sea (core GGC27, grey with squares Brunelle et al., 2010) and the subarctic North Pacific (core PC13, black with triangles). (c) this study's OSIW/bottom sediment oxygenation record based on *U. peregrina* ($\delta^{13}C_{Uvi}$) from northern shallow core 13 (violet) and northern deep core 79 (blue), both inverted for better comparison. (d) Fe concentration within the terrigenous fraction based on XRF-derived Fe/K ratios in southern Okhotsk Sea core 4 (red line). (e) Biogenic opal concentrations of Okhotsk Sea core 4 (this study, light brown with open circles) and Subarctic North Pacific core PC13 (light green line with filled diamonds, Brunelle et al., 2010). (f) atmospheric CO_2 concentrations from West Antarctic Ice Sheet Divide (WDC) ice core (Marcott et al., 2014). (For interpretation of the references to colour in this figure legend, the reader is referred to the web version of this article.)

depth (OSIW) water mass stratification during deglacial warm phases may have helped to load the OSIW during B/A ad PB with higher $Si(OH)_4$ concentrations from the deep ocean compared to today (Max et al., 2014; Sarmiento et al., 2004). Concurrent Fe maxima observed in all sediment records along the pathway of the southward-flowing ESC indicate that in addition the amount of lithogenic material increased within the OSIW, thus creating an "optimal nutrient mix" by adding iron to the sediment suspension. Even if the enhanced amount of terrigenous Fe provision to the suspension load of OSIW waters may have not become fully bio-available, a number of recent studies provided evidence that a close coupling exists on instrumental time scales between fluvial Amur Fe discharge and bio-available Fe in the pelagic subarctic Pacific and its marginal seas (Kanna et al., 2014; Lam and Bishop, 2008; Nishioka et al., 2014a, 2014b). Such higher (than modern) concentrations of suspended macronutrients together with Fe were further reinforced through the observed low primary production of biogenic silica within the Okhotsk Sea, especially during the B-A (Fig. 11e) likely caused by local stratification processes, e.g. due to high freshwater runoff (Okazaki et al., 2014; Riethdorf, 2013). In combination with maximum riverine supply such biogenic under-utilization probably further conserved $Si(OH)_4$ and bio-available Fe concentrations in the mid-depth, highly turbid, weakly ventilated water column. These OSIW masses may have thus contributed to the partial decoupling of silicate and nitrate-based isotope proxies in the WSAP during the Bølling-Allerød (Kohfeld and Chase, 2011; Maier et al., 2015). In addition to these hypothesized changes in the nutrient availability, stratification changes induced warm mixed layer maxima, which further fostered productivity maxima (Riethdorf et al., 2013).

Independent support for this scenario is provided by data from cores located in the southern Okhotsk Sea, distal from the immediate influence of local fluvial transport. There, maxima in terrigenous detrital OM accumulation supply were observed during the deglaciation (Okazaki et al., 2014; Ternois et al., 2001). The authors concluded that sea ice transport, fluvial supply by the Amur and continental debris from rising sea levels and inundated shallow shelf areas would all constitute likely causes. Combined with evidence from our productivity and OSIW ventilation data and the established modern oceanic transport mechanisms of suspended material in the turbid OSIW layer (Hansell, 2002; Nakatsuka et al., 2004a, 2004b), we suggest that OSIW acted as an efficient, lateral transport mechanism for nutrient export over wide distances into the open mid-depth North Pacific ocean. There, the low-O_2, and nutrient/Fe-enriched OSIW was upwelled into the upper mixed layer during wintertime turbulent mixing, in analogy to modern conditions (Nakatsuka et al., 2009; Nishioka et al., 2011) and facilitated the transient repletion of nutrients, including Fe, during the B/A and PB. Our hypothesis helps to explain the rather enigmatic pattern of higher-than-modern nutrient utilization during the deglacial productivity peaks throughout the subarctic NW-Pacific and its marginal seas based on nitrogen isotopes and other proxydata (Fig. 11b, Brunelle et al., 2007; Brunelle et al., 2010; Kohfeld and Chase, 2011; Okazaki et al., 2014). In addition, we presume that due to the observed ventilation minima in OSIW during the B/A and PB (Figs. 4 and 11c), denitrification was regionally enhanced, supporting a slightly elevated ^{d15}N OSIW signature (Fig. 11b, Yoshikawa et al., 2006). At the same time, the decreased O_2 content of OSIW and the northward-displaced circulation potentially fostered the establishment of oxygen minimum zones in the North Pacific Ocean, including northerly subarctic regions like the Bering Sea (Caissie et al., 2010; Kohfeld and Chase, 2011; Kuehn et al., 2014).

Lastly, though being a sink for atmospheric CO_2 today, as the subarctic Pacific constitutes one of the three main modern High Nutrient/Low Chlorophyll regions globally, transient Fe-replete conditions caused by lateral subsurface input would re-adjust the efficiency of the "biological pump" to more effective sequestration of atmospheric CO_2 into the deep ocean by better nutrient utilization and higher primary production. The last glacial termination's productivity spikes in the North Pacific (Crusius et al., 2004; Galbraith et al., 2007; Keigwin et al., 1992) likely contributed to shaping millennial-scale deglacial atmospheric CO_2 changes by a varying interplay between (1) release of old CO_2-rich deep water masses into the atmosphere and (2) a sequestration of CO_2 into the deep ocean through primary production and changes in the efficiency of carbon export from the upper ocean to the abyss (Galbraith et al., 2007). Notably, our timing of changes in OSIW biogeochemical and ventilation characteristics correlate both with a North Pacific maximum in nutrient utilization/export production, and a transient slowdown in the deglacial atmospheric CO_2 rise during the late phase of the Bølling-Allerød period (Fig. 11f, Marcott et al., 2014), i.e. after maximal releases of old carbon into the atmosphere as hypothesized earlier (Galbraith et al., 2007). Thus, intermediate water masses likely constitute important facilitators for larger regional-scale modulations in ocean biogeochemistry, with the potential to affect the deglacial global carbon cycle, warranting a more detailed understanding and future studies on both glacial-interglacial and shorter timescales.

6. Conclusions

We carried out a comprehensive multi-proxy-based reconstruction of Okhotsk Sea Intermediate Water ventilation and biogeochemical characteristics over the last glacial termination based on a set of high-resolution AMS ^{14}C-dated sediment cores. Based on ventilation ages and epibenthic stable carbon isotopes we have provided evidence that decreases in OSIW ventilation were largely driven by increases in organic matter content and remineralization rates, rather than changes in formation rates and overturning of OSIW in the Okhotsk Sea. From differences in ventilation ages between the northerly Okhotsk Sea and the southerly open Japan margin we deduce that OSIW influence on lower latitude subtropical North Pacific Intermediate Water waned during the during the warm Bølling-Allerød and Preboreal phases. These regional differences explain observed large scatter in earlier data compilations (Okazaki et al., 2010) and indicate more complex intermediate water circulation patterns than previously assumed, in analogy to recently observed, regionally differing surface and mixed layer hydrography during the last glacial termination (Max et al., 2012; Riethdorf et al., 2013). At the same time, OSIW was no source of oxygen for NPIW during the Bølling-Allerød, thus providing a positive feedback for basin-wide intensification of Oxygen Minimum Zones during the last glacial termination, in line with hypotheses that called for elevated respiration rates in the open North Pacific to decrease the O_2 content of NPIW (Crusius et al., 2004).

We observed millennial-scale OSIW ventilation decreases during deglacial warm periods to be in phase, with increases in terrigenous suspension load and deposition in the Okhotsk Sea. To some extent, terrigenous sediment was likely supplied by continental shelf flooding through eustatic sea-level rise, mainly during the early-mid deglacial (17–14 ka). However, we speculate that during the warm Allerød and Preboreal phases, marine productivity maxima on the Sakhalin margin, fuelled by iron- and nutrient-rich terrestrial material was mainly sourced from the Siberian hinterland and delivered via Amur freshwater discharge peaks. Support for this assumption of maxima in river runoff comes from the close correlation with deglacial increases in hinterland precipitation and heat transport linked to the northward propagation of the East

Asian Summer, which were conceivably linked to widespread deglacial thawing of Siberian permafrost in the vast Amur catchment area. Likely, such melting mobilized significant amounts of terrigenous organic matter and detritus that was transported from the catchment into the Okhotsk Sea basin, where it in turn fostered OSIW oxygenation decreases through maxima in respiration processes, while increasing the dissolved and particulate nutrient loads in mid-depth waters. This closely coupled continent-ocean system thus provides an example for low-latitude East Asian monsoon forcing exerting an influence on mid-latitude and subarctic North Pacific oceanography and marine biogeochemistry.

We suggest that correlation of the observed ventilation minima with maxima in primary productivity and nutrient utilization in the open North Pacific implies an increase of OSIW-sourced lateral transport of macronutrients and iron into the subarctic North Pacific during the Bølling-Allerød and Preboreal. Variations in this export mechanism have presumably contributed to pelagic productivity peaks and simultaneously lead to a higher utilization of nutrients than observed today during deglacial warm phases. In the subarctic North Pacific region, this scenario would have temporarily relieved the upper ocean from micronutrient limiting conditions. The upwelling of the mid-depth nutrient-enriched OSIW during wintertime mixing likely switched the region to a transient, more efficient CO_2 sink during the Bølling-Allerød and Preboreal, two intervals that are marked by a slowdown in atmospheric CO2 rise.

Authors' contributions

LLJ measured and compiled data, and wrote paper. LLJ, RT and DN designed study and measured isotope data. RK measured opal and XRF on core 4, UK carried out freshwater algae analyses analyses, LM contributed to isotope and AMS ^{14}C data, UR contributed XRF measurements, SG provided samples and data. All authors participated in the discussion of results and conclusions and contributed to the final version of the paper.

Acknowledgements

We acknowledge the professional support and dedication of masters and crews of R/V Akademik Lavrentiev and R/V Sonne on expeditions LV28, LV29 and SO178. We thank J. Heinze and B. Fessler for help in sample analysis; and N. Stange, M. Zygmuntowski and A. Dix for their support in sediment sampling and processing. The material for this study and initial works were carried out within frameworks of the German-Russian KOMEX projects (1998–2006). We acknowledge funds provided by the German Ministry for Research and Education (BMBF) under the grant No. 03F0704 (SIGEPAX) as well as financial support by the AWI and the Helmholtz REKLIM Initiative. UK acknowledges funding by the VILLUM Foundation (grant no. 10100).

Appendix A. Supplementary data

Supplementary data related to this article can be found at http://dx.doi.org/10.1016/j.quascirev.2017.01.016.

References

Addison, J.A., Finney, B.P., Dean, W.E., Davies, M.H., Mix, A.C., Stoner, J.S., Jaeger, J.M., 2012. Productivity and sedimentary δ15N variability for the last 17,000 years along the northern Gulf of Alaska continental slope. Paleoceanography 27.

Ahagon, N., Ohkushi, K., Uchida, M., Mishima, T., 2003. Mid-depth circulation in the northwest Pacific during the last deglaciation: evidence from foraminiferal radiocarbon ages. Geophys. Res. Lett. 30, 2097.

Ahagon, N., Uchida, M., 2004. Transient response of mid-depth circulation in the northwest Pacific around the younger Dryas event inferred from AMS C-14 ages of foraminifera. Nucl. Instrum. Methods Phys. Res. Sect. B - Beam Interact. Mater. Atom 223, 466–470.

Barker, S., Knorr, G., Vautravers, M.J., Diz, P., Skinner, L.C., 2010. Extreme deepening of the Atlantic overturning circulation during deglaciation. Nat. Geosci. 3, 567–571.

Bauch, D., Erlenkeuser, H., Winckler, G., Pavlova, G., Thiede, J., 2002. Carbon isotopes and habitat of polar planktic foraminifera in the Okhotsk Sea: the 'carbonate ion effect' under natural conditions. Mar. Micropaleontol. 45, 83–99.

Bazarova, V.B., Klimin, M.A., Mokhova, L.M., Orlova, L.A., 2008. New pollen records of late Pleistocene and Holocene changes of environment and climate in the lower Amur river basin, NE Eurasia. Quat. Int. 179, 9–19.

Biebow, N., Hütten, E., 1999. Cruise Reports KOMEX I and II: RV Professor Gagarinsky Cruise 22, RV Akademik M.A. Lavrentyev Cruise 28, GEOMAR Report. GEOMAR Research Centre for Marine Geosciences, Kiel, p. 188.

Biebow, N., Kulinich, R., Baranov, B., 2002. KOMEX II, Kurile Okhotsk Sea Marine Experiment: Cruise Report RV Akademik M.A. Lavrentyev Cruise 29, Leg 1 and Leg 2. GEOMAR Forschungszentrum für Marine Geowissenschaften, Kiel.

Blaauw, M., 2010. Methods and code for "classical" age-modelling of radiocarbon sequences. Quat. Geochronol. 5, 512–518.

Blaauw, M., Andres Christen, J., 2011. Flexible Paleoclimate age-depth models using an autoregressive gamma process. Bayesian Anal. 6, 457–474.

Blaauw, M., Bennett, K.D., Christen, J.A., 2010. Random walk simulations of fossil proxy data. Holocene 20, 645–649.

Blockley, S.P.E., Blaauw, M., Ramsey, C.B., van der Plicht, J., 2007. Building and testing age models for radiocarbon dates in Lateglacial and Early Holocene sediments. Quat. Sci. Rev. 26, 1915–1926.

Broecker, W.S., 1991. The great ocean conveyor. Oceanography 4, 79–89.

Brunelle, B.G., Sigman, D.M., Cook, M.S., Keigwin, L.D., Haug, G.H., Plessen, B., Schettler, G., Jaccard, S.L., 2007. Evidence from diatom-bound nitrogen isotopes for subarctic Pacific stratification during the last ice age and a link to North Pacific denitrification changes. Paleoceanography 22, PA1215.

Brunelle, B.G., Sigman, D.M., Jaccard, S.L., Keigwin, L.D., Plessen, B., Schettler, G., Cook, M.S., Haug, G.H., 2010. Glacial/interglacial changes in nutrient supply and stratification in the western subarctic North Pacific since the penultimate glacial maximum. Quat. Sci. Rev. 29, 2579–2590.

Bubenshchikova, N., Nuernberg, D., Lembke-Jene, L., Pavlova, G., 2008. Living benthic foraminifera of the Okhotsk Sea: faunal composition, standing stocks and microhabitats. Mar. Micropaleontol. 69, 314–333.

Bubenshchikova, N.V., Nuernberg, D., Gorbarenko, S.A., Lembke-Jene, L., 2010. Variations of the oxygen minimum zone of the Okhotsk sea during the last 50 ka as indicated by benthic foraminiferal and biogeochemical data. Okeanologiya 50, 93–106.

Caissie, B.E., Brigham-Grette, J., Lawrence, K.T., Herbert, T.D., Cook, M.S., 2010. Last Glacial maximum to Holocene sea surface conditions at Umnak Plateau, Bering Sea, as inferred from diatom, alkenone, and stable isotope records. Paleoceanography 25, PA1206.

Chebykin, E.P., Gorbarenko, S.A., Stepanova, O.G.G., Panov, V.S., Goldberg, E.L., 2015. Geochemical multi-element signatures of glacial and interglacial facies of the Okhotsk Sea deep-water sediments during the past 350 kyr: a response to global climate changes at the orbital and millennial scales. Paleoceanography 30, 303–316.

Chlachula, J., 2003. The Siberian loess record and its significance for reconstruction of Pleistocene climate change in north-central Asia. Quat. Sci. Rev. 22, 1879–1906.

Cook, M.S., Keigwin, L.D., 2014. Radiocarbon profiles of the NW Pacific from the LGM and deglaciation: evaluating ventilation metrics and the effect of uncertain surface reservoir ages. Paleoceanography n/a-n/a.

Cook, M.S., Keigwin, L.D., Sancetta, C.A., 2005. The deglacial history of surface and intermediate water of the Bering Sea. Deep Sea Res. Part II Top. Stud. Oceanogr. 52, 2163–2173.

Craig, H., 1957. Isotopic standards for carbon and oxygen and correction factors for mass-spectrometric analysis of carbon dioxide. Geochimica Cosmochimica Acta 12, 133–149.

Crusius, J., Pedersen, T., Kienast, S., Keigwin, L., Labeyrie, L., 2004. Influence of northwest Pacific productivity on North Pacific intermediate water oxygen concentrations during the Bøling-Ållerød interval (14.7–12.9 ka). Geology 32, 633–636.

Davies, M.H., Mix, A.C., Stoner, J.S., Addison, J.A., Jaeger, J., Finney, B., Wiest, J., 2011. The deglacial transition on the southeastern Alaska Margin: meltwater input, sea level rise, marine productivity, and sedimentary anoxia. Paleoceanography 26, PA2223.

Dean, W.E., Zheng, Y., Ortiz, J.D., Van Geen, A., 2006. Sediment Cd and Mo accumulation in the oxygen-minimum zone off western Baja California linked to global climate over the past 52 kyr. Paleoceanography 21, PA4209.

del Giorgio, P., Duarte, C., 2002. Respiration in the open ocean. Nature 420, 379–384.

DeMaster, D.J., 1981. Measuring biogenic silica in marine sediments and suspended matter. In: Hurd, D.C., Spenser, D.W. (Eds.), Marine Particles: Analysis and Characterization. American Geophysical Union, Washington, D. C., pp. 363–368

Duce, R.A., Tindale, N.W., 1991. Atmospheric transport of iron and its deposition in the ocean. Limnol. Oceanogr. 36, 1715–1726.

Dullo, W., Biebow, N., 2004. SO178-KOMEX Cruise Report: Mass Exchange Processes and Balances in the Okhotsk Sea. IFM-GEOMAR Report. IFM-GEOMAR, Kiel.

Duplessy, J., Arnold, M., Bard, E., Juillet-Leclerc, A., Kallel, N., Labeyrie, L., 1989. AMS

C-14 study of transient events and of the ventilation rate of the Pacific intermediate water during the last deglaciation. Radiocarbon 31, 493–502.
Dykoski, C., Edwards, R., Cheng, H., Yuan, D., Cai, Y., Zhang, M., Lin, Y., Qing, J., An, Z., Revenaugh, J., 2005. A high-resolution, absolute-dated Holocene and deglacial Asian monsoon record from Dongge Cave, China. Earth Planet. Sci. Lett. 233, 71–86.
Emerson, S., Watanabe, Y.W., Ono, T., Mecking, S., 2004. Temporal trends in apparent oxygen utilization in the upper pycnocline of the North Pacific: 1980–2000. J. Oceanogr. 60, 139–147.
Emile-Geay, J., Cane, M., Naik, N., Seager, R., Clement, A., Van Geen, A., 2003. Warren revisited: atmospheric freshwater fluxes and "why is no deep water formed in the North Pacific. J. Geophys. Res. Ocean 108, 3178.
Fukamachi, Y., Shirasawa, K., Polomoshnov, A.M., Ohshima, K.I., Kalinin, E., Nihashi, S., Melling, H., Mizuta, G., Wakatsuchi, M., 2009. Direct observations of sea-ice thickness and brine rejection off Sakhalin in the Sea of Okhotsk. Cont. Shelf Res. 29, 1541–1548.
Galbraith, E.D., Jaccard, S.L., Pedersen, T.F., Sigman, D.M., Haug, G.H., Cook, M., Southon, J.R., Francois, R., 2007. Carbon dioxide release from the North Pacific abyss during the last deglaciation. Nature 449, 890–U899.
Galbraith, E.D., Kienast, M., Jaccard, S.L., Pedersen, T.F., Brunelle, B.G., Sigman, D.M., Kiefer, T., 2008. Consistent relationship between global climate and surface nitrate utilization in the western subarctic Pacific throughout the last 500 ka. Paleoceanography 23, PA2212.
Garcia, H.E., Locarnini, R.A., Boyer, T.P., Antonov, J.I., Baranova, O.K., Zweng, M.M., Johnson, D.R., 2010a. World Ocean Atlas 2009, Volume 3: Dissolved Oxygen, Apparent Oxygen Utilization, and Oxygen Saturation. U.S. Government Printing Office, Washington, D.C.
Garcia, H.E., Locarnini, R.A., Boyer, T.P., Antonov, J.I., Baranova, O.K., Zweng, M.M., Johnson, D.R., 2010b. World Ocean Atlas 2009, Volume 4: Nutrients (Phosphate, Nitrate, Silicate). U.S. Government Printing Office, Washington, D.C.
Gebhardt, H., Sarnthein, M., Grootes, P.M., Kiefer, T., Kuehn, H., Schmieder, F., Röhl, U., 2008. Paleonutrient and productivity records from the subarctic North Pacific for Pleistocene glacial terminations I to V. Paleoceanography 23, PA4212.
Goes, J.I., Gomes, H.D.R., Limsakul, A., Saino, T., 2004. The influence of large-scale environmental changes on carbon export in the North Pacific Ocean using satellite and shipboard data. Deep Sea Res. Part II Top. Stud. Oceanogr. 51, 247–279.
Goldberg, E., Gorbarenko, S., Shaporenko, A., Phedorin, M., Artemova, A., Bosin, A., Zolotarev, K., 2005. SRXFA for element compositions of bottom sediments from the Okhotsk Sea. Nucl. Instrum. Methods Phys. Res. Sect. A Accel. Spectrom. Detect. Assoc. Equip. 543, 280–283.
Gorbarenko, S., Khusid, T.A., Basov, I., Oba, T., Southon, J., Koizumi, I., 2002. Glacial Holocene environment of the southeastern Okhotsk Sea: evidence from geochemical and palaeontological data. Palaeogeogr. Palaeoclimatol. Palaeoecol. 177, 237–263.
Gorbarenko, S., Southon, J., Keigwin, L., Cherepanova, M., Gvozdeva, I., 2004. Late Pleistocene-Holocene oceanographic variability in the Okhotsk Sea: geochemical, lithological and paleontological evidence. Palaeogeogr. Palaeoclimatol. Palaeoecol. 209, 281–301.
Gorbarenko, S.A., Goldberg, E.L.A.V., Kashgarian, M., Velivetskaya, T.A.Y.A., Zakharkov, S.P., Pechnikov, V.S., Bosin, A.A.A.E., Psheneva, O.Y.A.E., Ivanova, E.D., 2007. Millennium scale environment changes of the Okhotsk sea during last 80 kyr and their phase relationship with global climate changes. J. Oceanogr. 63, 609–623.
Gorbarenko, S.A., Harada, N., Malakhov, M.I., Vasilenko, Y.P., Bosin, A.A., Gol'dberg, E.L., 2008. Millennial-scale climatic and environmental oscillations in the Sea of Okhotsk in response to global changes during the last 190 Ka. Dokl. Earth Sci. 423, 1410–1413.
Gorbarenko, S.A., Harada, N., Malakhov, M.I., Velivetskaya, T.A., Vasilenko, Y.P., Bosin, A.A., Derkachev, A.N., Goldberg, E.L., d, A.V.I., 2012. Responses of the Okhotsk Sea environment and sedimentology to global climate changes at the orbital and millennial scale during the last 350 kyr. Deep Sea Res. II 61–64, 73–84.
Gorbarenko, S.A., Psheneva, O.Y., Artemova, A.V., Matul, A.G., Tiedemann, R., Nuernberg, D., 2010. Paleoenvironment changes in the NW Okhotsk Sea for the last 18 kyr determined with micropaleontological, geochemical, and lithological data. Deep Sea Res. Part I Oceanogr. Res. Pap. 57, 797–811.
Hansell, D.A., 2002. Dissolved organic carbon export with North Pacific intermediate water formation. Glob. Biogeochem. Cycle 16, 1007.
Harada, N., Sato, M., Sakamoto, T., 2008. Freshwater impacts recorded in tetraunsaturated alkenones and alkenone sea surface temperatures from the Okhotsk Sea across millennial-scale cycles. Paleoceanography 23, PA3201.
Harada, N., Sato, M., Seki, O., Timmermann, A., 2012. Sea surface temperature changes in the Okhotsk Sea and adjacent North Pacific during the last glacial maximum and deglaciation. Deep Sea Res. II Top. Stud. Oceanogr. 61–64, 93–105.
Harrison, P.J., Whitney, F.A., Tsuda, A., Saito, H., Tadokoro, K., 2004. Nutrient and plankton dynamics in the NE and NW Gyres of the subarctic pacific ocean. J. Oceanogr. 60, 93–117.
Herguera, J., Peltzer, E., Brewer, P., 2009. Benthic foraminifera habitats and carbon isotopes: new perspective from thermodynamic constrains on intermediate waters respiration. Geophys. Res. Abstr. 11, EGU2009–3831, 2009 EGU General Assembly 2009.
Ikehara, K., Ohkushi, K.A.I., Shibahara, A., Hoshiba, M., 2006. Change of bottom water conditions at intermediate depths of the Oyashio region, NW Pacific over the past 20,000 yrs. Glob. Planet. Change 53, 78–91.
Inagaki, M., Yamamoto, M., Igarashi, Y., Ikehara, K., 2009. Biomarker records from core GH02-1030 off Tokachi in the northwestern Pacific over the last 23,000 years: environmental changes during the last deglaciation. J. Oceanogr. 65, 847–858.
Itaki, T., Kim, S., Rella, S.F., Uchida, M., Tada, R., Khim, B.-K., 2012. Millennial-scale variations of late Pleistocene radiolarian assemblages in the Bering Sea related to environments in shallow and deep waters. Deep Sea Res. Part II Top. Stud. Oceanogr. 61–64, 127–144.
Itou, M., Ono, T., Noriki, S., 2003. Provenance of intermediate waters in the western North Pacific deduced from thermodynamic imprint on delta C-13 of DIC. J. Geophys. Res. Ocean 108, 3347.
Jaccard, S.L., Galbraith, E., 2013. Direct ventilation of the North Pacific did not reach the deep ocean during the last deglaciation. Geophys. Res. Lett. 40, 199–203.
Jaccard, S.L., Galbraith, E.D., 2011. Large climate-driven changes of oceanic oxygen concentrations during the last deglaciation. Nat. Geosci. 5, 151–156.
Jaccard, S.L., Galbraith, E.D., Sigman, D.M., Haug, G.H., 2010. A pervasive link between Antarctic ice core and subarctic Pacific sediment records over the past 800 kyrs. Quat. Sci. Rev. 29, 206–212.
Jaccard, S.L., Galbraith, E.D., Sigman, D.M., Haug, G.H., Francois, R., Pedersen, T.F., Dulski, P., Thierstein, H.R., 2009. Subarctic Pacific evidence for a glacial deepening of the oceanic respired carbon pool. Earth Planet. Sci. Lett. 277, 156–165.
Jaccard, S.L., Haug, G.H., Sigman, D., Pedersen, T., Thierstein, H., Rohl, U., 2005. Glacial/interglacial changes in subarctic North Pacific stratification. Sci. (New York, NY) 308, 1003–1006.
Jansen, J.H.F., Van der Gaast, S.J., Koster, B., Vaars, A.J., 1998. CORTEX, a shipboard XRF-scanner for element analyses in split sediment cores. Mar. Geol. 151, 143–153.
Kanna, N., Toyota, T., Nishioka, J., 2014. Iron and macro-nutrient concentrations in sea ice and their impact on the nutritional status of surface waters in the southern Okhotsk Sea. Prog. Oceanogr. 126, 44–57.
Keigwin, L., Jones, G., Froelich, P., 1992. A 15,000 year paleoenvironmental record from Meiji Seamount, far northwestern Pacific. Earth Planet. Sci. Lett. 111, 425–440.
Khim, B., Sakamoto, T., 2012. Reconstruction of surface water conditions in the central region of the Okhotsk Sea during the last 180 kyrs. Deep Sea Res. Part II Top. Stud. Oceanogr. 61–64, 63–72.
Kienast, S., Hendy, I., Crusius, J., Pedersen, T., Calvert, S., 2004. Export production in the subarctic North Pacific over the last 800 kyrs: no evidence for iron fertilization? J. Oceanogr. 60, 189–203.
Kitani, K., 1973. An oceanographic study of the Okhotsk Sea - particularly in regard to cold waters. Bull. Far Sear Fish. Res. Lab. 9, 45–76.
Klinkhammer, G.P., Mix, A.C., Haley, B.A., 2009. Increased dissolved terrestrial input to the coastal ocean during the last deglaciation. Geochem. Geophys. Geosys. 10, Q3009.
Kohfeld, K.E., Chase, Z., 2011. Controls on deglacial changes in biogenic fluxes in the North Pacific Ocean. Quat. Sci. Rev. 30, 3350–3363.
Kokfelt, U., 2003. An Analysis of Pollen, Spores and Chlorophycean Algae from the Sea of Okhotsk: Implications for Late Glacial and Holocene Climatic Change. Geomar & Geologisk Museum Copenhagen, Copenhagen, Kiel, p. 56.
Kuehn, H., Lembke-Jene, L., Gersonde, R., Esper, O., Lamy, F., Arz, H., Kuhn, G., Tiedemann, R., 2014. Laminated sediments in the Bering Sea reveal atmospheric teleconnections to Greenland climate on millennial to decadal timescales during the last deglaciation. Clim. Past 10, 2215–2236.
Kuzmin, Y.V., Burr, G.S., Gorbunov, S.V., Rakov, V.A., Razjigaeva, N.G., 2007. A tale of two seas: reservoir age correction values (R, Delta R) for the Sakhalin Island (Sea of Japan and Okhotsk Sea). Nucl. Instrum. Methods Phys. Res. Sect. B Beam Interact. Mater. Atom 259, 460–462.
Lam, P.J., Bishop, J.K.B., 2008. The continental margin is a key source of iron to the HNLC North Pacific Ocean. Geophys. Res. Lett. 35, L07608.
Lam, P.J., Robinson, L.F., Blusztajn, J., Li, C., Cook, M.S., McManus, J.F., Keigwin, L.D., 2013. Transient stratification as the cause of the North Pacific productivity spike during deglaciation. Nat. Geosci.
Lembke-Jene, L., 2013. Millennial-scale Changes of Intermediate Water Ventilation, Productivity and Nutrient Supply in the Okhotsk Sea and Subarctic North Pacific during the Last 18,000 Years. Fachbereich Geowissenschaften. Universität Bremen, Bremen, p. 202.
Ludmann, T., Wong, H., 2003. Characteristics of gas hydrate occurrences associated with mud diapirism and gas escape structures in the northwestern Sea of Okhotsk. Mar. Geol. 201, 269–286.
Lutze, G.F., Thiel, H., 1989. Epibenthic foraminifera from elevated microhabitats; Cibicidoides wuellerstorfi and Planulina ariminensis. J. Foraminifer. Res. 19, 153–158.
Mahowald, N., Baker, A., Bergametti, G., Brooks, N., Duce, R., Jickells, T., Kubilay, N., Prospero, J., Tegen, I., 2005. Atmospheric global dust cycle and iron inputs to the ocean. Glob. Biogeochem. Cycle 19.
Maier, E., Méheust, M., Abelmann, A., Gersonde, R., Chapligin, B., Ren, J., Stein, R., Meyer, H., Tiedemann, R., 2015. Deglacial subarctic Pacific surface water hydrography and nutrient dynamics and links to North Atlantic climate variability and atmospheric CO2. Paleoceanography 30, 949–968.
Marcott, S.A., Bauska, T.K., Buizert, C., Steig, E.J., Rosen, J.L., Cuffey, K.M., Fudge, T.J., Severinghaus, J.P., Ahn, J., Kalk, M.L., McConnell, J.R., Sowers, T.A., Taylor, K.C., White, J.W.C., Brook, E.J., 2014. Centennial-scale changes in the global carbon cycle during the last deglaciation. Nature 514, 616–619.
Matthiessen, J., Brenner, W., 1996. Chlorococcalalgen und Dinoflagellaten-Zysten in

rezenten Sedimenten des Greifswalder Boddens (südliche Ostsee). Senckenberg. Maritima 27, 33–48.
Matthiessen, J., Kunz-Pirrung, M., Mudie, P.J., 2000. Freshwater chlorophycean algae in recent sediments of the Beaufort, Laptev and Kara Seas (Arctic Ocean) as indicators of river runoff. Int. J. Earth Sci. 89, 470–485.
Max, L., Lembke-Jene, L., Riethdorf, J.-R., Tiedemann, R., Nürnberg, D., 2014. Pulses of enhanced north Pacific intermediate water ventilation from the Okhotsk sea and Bering sea during the last deglaciation. Clim. Past 10, 591–605.
Max, L., Riethdorf, J.-R., Tiedemann, R., Smirnova, M., Lembke-Jene, L., Fahl, K., Nürnberg, D., Matul, A., Mollenhauer, G., 2012. Sea surface temperature variability and sea-ice extent in the subarctic northwest Pacific during the past 15,000 years. Paleoceanography 27, PA3213.
McCorkle, D., Corliss, B., Farnham, C., 1997. Vertical distributions and stable isotopic compositions of live (stained) benthic foraminifera from the North Carolina and California continental margins. Deep Sea Res. Part I Oceanogr. Res. Pap. 44, 983–1024.
McCorkle, D.C., Keigwin, L.D., 1994. Depth profiles of δ 13C in bottom water and core top C. wuellerstorfi on the Ontong Java Plateau and Emperor Seamounts. Paleoceanography 9, 197–208.
McKay, J., Pedersen, T., Kienast, S., 2004. Organic carbon accumulation over the last 16 kyr off Vancouver Island, Canada: evidence for increased marine productivity during the deglacial. Quat. Sci. Rev. 23, 261–281.
McManus, J.F., Francois, R., Gherardi, J.-M., Keigwin, L.D., Brown-Leger, S., 2004. Collapse and rapid resumption of Atlantic meridional circulation linked to deglacial climate changes. Nature 428, 834–837.
Misumi, K., Tsumune, D., Yoshida, Y., Uchimoto, K., Nakamura, T., Nishioka, J., Mitsudera, H., Bryan, F.O., Lindsay, K., Moore, J.K., Doney, S.C., 2011. Mechanisms controlling dissolved iron distribution in the North Pacific: a model study. J. Geophys. Res. 116, G03005.
Mix, A., Lund, D., Pisias, N., Boden, P., Bornmalm, L., Lyle, M., Pike, J., 1999. Rapid climate oscillations in the northeast Pacific during the last deglaciation reflect Northern and Southern Hemisphere sources. Mech. Glob. Clim. Change Millenn. Time Scales 112, 127–148.
Müller, P.J., Schneider, R., 1993. An automated leaching method for the determination of opal in sediments and particulate matter. Deep Sea Res. Part I Oceanogr. Res. Pap. 40, 425–444.
Nadeau, M.-J., Grootes, P.M., Schleicher, M., Hasselberg, P., Rieck, A., Bitterling, M., 1998. Sample throughput and data quality at the Leibniz-Labor AMS facility. Radiocarbon 40 (1), 239–245.
Nadeau, M.-J., Schleicher, M., Grootes, P.M., Erlenkeuser, H., Gottdang, A., Mous, D.J.W., Sarnthein, M., Willkomm, H., 1997. The Leibniz-Labor AMS facility at the Christian-Albrechts University, Kiel, Germany. Nucl. Instrum. Methods Phys. Res. Sect. B 123, 22–30.
Nakatsuka, T., Fujimune, T., Yoshikawa, C., Noriki, S., Kawamura, K., Fukamachi, Y., Mizuta, G., Wakatsuchi, M., 2004a. Biogenic and lithogenic particle fluxes in the western region of the Sea of Okhotsk: implications for lateral material transport and biological productivity. J. Geophys. Res. Ocean 109, C09S13.
Nakatsuka, T., Nishioka, J., Shiraiwa, T., Project, a.m.o.t.A.-O., 2009. Biogeochemical linkage between Amur River basin and western subarctic Pacific by iron transport through Okhotsk Sea intermediate water: a new paradigm to explain changes in ocean primary productivity. PICES Sci. Rep. 48.
Nakatsuka, T., Toda, M., Kawamura, K., Wakatsuchi, M., 2004b. Dissolved and particulate organic carbon in the Sea of Okhotsk: transport from continental shelf to ocean interior. J. Geophys. Res. Ocean 109, C09S14.
Nakatsuka, T., Yoshikawa, C., Toda, M., Kawamura, K., Wakatsuchi, M., 2002. An extremely turbid intermediate water in the Sea of Okhotsk: implication for the transport of particulate organic matter in a seasonally ice-bound sea. Geophys. Res. Lett. 29, 1757.
Nishioka, J., Mitsudera, H., Yasuda, I., Liu, H., Nakatsuka, T., Volkov, Y.N., 2014a. Biogeochemical and physical processes in the Sea of Okhotsk and the linkage to the Pacific ocean. Prog. Oceanogr. 126, 1–7.
Nishioka, J., Nakatsuka, T., Ono, K., Volkov, Y.N., Scherbinin, A., Shiraiwa, T., 2014b. Quantitative evaluation of iron transport processes in the Sea of Okhotsk. Prog. Oceanogr. 126, 180–193.
Nishioka, J., Ono, T., Saito, H., Nakatsuka, T., Takeda, S., Yoshimura, T., Suzuki, K., Kuma, K., Nakabayashi, S., Tsumune, D., Mitsudera, H., Johnson, W.K., Tsuda, A., 2007. Iron supply to the western subarctic Pacific: importance of iron export from the Sea of Okhotsk. J. Geophys. Res. Ocean 112, C10012.
Nishioka, J., Ono, T., Saito, H., Sakaoka, K., Yoshimura, T., 2011. Oceanic iron supply mechanisms which support the spring diatom bloom in the Oyashio region, western subarctic Pacific. J. Geophys. Res. Ocean 116, C02021.
Nishioka, J., Takeda, S., Kudo, I., Tsumune, D., Yoshimura, T., Kuma, K., Tsuda, A., 2003. Size-fractionated iron distributions and iron-limitation processes in the subarctic NW Pacific. Geophys. Res. Lett. 30, 1730.
Nürnberg, D., Dethleff, D., Tiedemann, R., Kaiser, A., Gorbarenko, S.A., 2011. Okhotsk Sea ice coverage and Kamchatka glaciation over the last 350ka — evidence from ice-rafted debris and planktonic δ18O. Palaeogeogr. Palaeoclimatol. Palaeoecol. 310, 191–205.
Nürnberg, D., Tiedemann, R., 2004. Environmental change in the Sea of Okhotsk during the last 1.1 million years. Paleoceanography 19, PA4011.
Ogi, M., Tachibana, Y., Nishio, F., Danchenkov, M., 2001. Does the fresh water supply from the Amur river flowing into the sea of Okhotsk affect sea ice formation? J. Meteorol. Soc. Jpn. 79, 123–129.
Ohkushi, K., 2004. Glacial intermediate water ventilation in the northwestern Pacific based on AMS radiocarbon dating. Nucl. Instrum. Methods Phys. Res. Sect. B Beam Interact. Mater. Atom 223–224, 460–465.
Ohkushi, K., Itaki, T., Nemoto, N., 2003. Last glacial-Holocene change in intermediate-water ventilation in the northwestern Pacific. Quat. Sci. Rev. 22, 1477–1484.
Okazaki, Y., Kimoto, K., Asahi, H., Sato, M., Nakamura, Y., Harada, N., 2014. Glacial to deglacial ventilation and productivity changes in the southern Okhotsk Sea. Palaeogeogr. Palaeoclimatol. Palaeoecol. 395, 53–66.
Okazaki, Y., Sagawa, T., Asahi, H., Horikawa, K., Onodera, J., 2012. Ventilation changes in the western North Pacific since the last glacial period. Clim. Past 8, 17–24.
Okazaki, Y., Timmermann, A., Menviel, L., Harada, N., Abe-Ouchi, A., Chikamoto, M.O., Mouchet, A., Asahi, H., 2010. Deepwater formation in the north Pacific during the last glacial termination. Science 329, 200–204.
Peterse, F., Prins, M.A., Beets, C.J., Troelstra, S.R., Zheng, H., Gu, Z., Schouten, S., Damste, J.S.S., 2011. Decoupled warming and monsoon precipitation in East Asia over the last deglaciation. Earth Planet. Sci. Lett. 301, 256–264.
Piotrowski, A.M., Goldstein, S.L., Hemming, S.R., Fairbanks, R.G., 2004. Intensification and variability of ocean thermohaline circulation through the last deglaciation. Earth Planet. Sci. Lett. 225, 205–220.
Rasmussen, S.O., Seierstad, I.K., Andersen, K.K., Bigler, M., Dahl-Jensen, D., Johnsen, S.J., 2008. Synchronization of the NGRIP, GRIP, and GISP2 ice cores across MIS 2 and palaeoclimatic implications. Quat. Sci. Rev. 27, 18–28.
Reid, J.L., 1965. Intermediate Waters of the Pacific Ocean, the Johns Hopkins Oceanographic Studies. The Johns Hopkins Press, Baltimore, pp. 1–85.
Reimer, P.J., Baillie, M.G.L., Bard, E., Bayliss, A., Beck, J.W., Blackwell, P.G., Ramsey, C.B., Buck, C.E., Burr, G.S., Edwards, R.L., Friedrich, M., Grootes, P.M., Guilderson, T.P., Hajdas, I., Heaton, T.J., Hogg, A.G., Hughen, K.A., Kaiser, K.F., Kromer, B., McCormac, F.G., Manning, S.W., Reimer, R.W., Richards, D.A., Southon, J.R., Talamo, S., Turney, C.S.M., van der Plicht, J., Weyhenmeye, C.E., 2009. INTCAL09 and MARINE09 radiocarbon age calibration curves, 0-50,000 years cal. BP. Radiocarbon 51, 1111–1150.
Richter, T.O., van der Gaast, S., Koster, B., Vaars, A., Gieles, R., de Stigter, H.C., De Haas, H., van Weering, T.C.E., 2006. The Avaatech XRF core scanner: technical description and applications to NE Atlantic sediments. In: Rothwell, R.G. (Ed.), New Techniques in Sediment Core Analysis. Geological Society, Special Publications, London, pp. 39–50.
Riethdorf, J.-R., Max, L., Nürnberg, D., Lembke-Jene, L., Tiedemann, R., 2013. Deglacial history of (sub) sea surface temperatures and salinity in the subarctic NW Pacific: implications for upper-ocean stratification. Paleoceanography 28, 91–104.
Riethdorf, J.R., 2012. Late Pleistocene to Holocene changes in Upper-ocean Stratification and Its Impact on Marine Productivity, Sea Surface Temperatures, and Salinity in the Subarctic Northwest Pacific. Mathematisch-Naturwissenschaftliche Fakultät. Christian-Albrechts-Universität zu Kiel, Kiel, p. 181.
Röhl, U., Abrams, L.J., 2000. High-resolution, downhole, and nondestructive core measurements from Sites 999 and 1001 in the Caribbean Sea: application to the Late Paleocene thermal maximum. In: Leckie, R.M., Sigurdsson, H., Acton, G.D., Draper, G. (Eds.), Proceedings of the Ocean Drilling Program, Scientific Results, College Station, TX (Ocean Drilling Program). Ocean Drilling Program, College Station, TX.
Rohling, E.J., Grant, K., Bolshaw, M., Roberts, A.P., Siddall, M., Hemleben, C., Kucera, M., 2009. Antarctic temperature and global sea level closely coupled over the past five glacial cycles. Nat. Geosci. 2, 500–504.
Sagawa, T., Ikehara, K., 2008. Intermediate water ventilation change in the subarctic northwest Pacific during the last deglaciation. Geophys. Res. Lett. 35, L24702.
Sakaguchi, Y., 1992. Cooling around 9000 BP caused by permafrost melt water burst. Bull. Dept. Geogr. Univ. Tokyo 24, 1–6.
Sakamoto, T., Ikehara, M., Aoki, K., Iijima, K., Kimura, N., Nakatsuka, T., Wakatsuchi, M., 2005. Ice-rafted debris (IRD)-based sea-ice expansion events during the past 100kyrs in the Okhotsk Sea. Deep Sea Res. Part II Top. Stud. Oceanogr. 52, 2275–2301.
Sarmiento, J.L., Gruber, N., Brzezinski, M.A., Dunne, J.P., 2004. High-latitude controls of thermocline nutrients and low latitude biological productivity. Nature 427, 56–60.
Sarnthein, M., Grootes, P.M., Kennett, J.P., Nadeau, M., Schmittner, A., Chiang, J., Hemming, S., 2007. 14C reservoir ages show deglacial changes in ocean currents and carbon cycle. In: Schmittner, A., Chiang, J.C.H., Hemming, S.R. (Eds.), Ocean Circulation: Mechanisms and Impacts, AGU Geophysical Monograph Series. American Geophysical Union, Washington, D.C, pp. 175–196.
Schlitzer, R., 2002. Interactive analysis and visualization of geoscience data with ocean data view. Comput. Geosci. 28, 1211–1218.
Seki, O., Harada, N., Sato, M., Kawamura, K., Ijiri, A., Nakatsuka, T., 2012. Assessment for paleoclimatic utility of terrestrial biomarker records in the Okhotsk Sea sediments. Deep Sea Res. Part II Top. Stud. Oceanogr. 61–64, 85–92.
Seki, O., Ikehara, M., Kawamura, K., Nakatsuka, T., Ohnishi, K., Wakatsuchi, M., Narita, H., Sakamoto, T., 2004. Reconstruction of paleoproductivity in the Sea of Okhotsk over the last 30 kyr. Paleoceanography 19, PA1016.
Seki, O., Kawamura, K., Nakatsuka, T., Ohnishi, K., Ikehara, M., Wakatsuchi, M., 2003. Sediment core profiles of long-chain n-alkanes in the Sea of Okhotsk: enhanced transport of terrestrial organic matter from the last deglaciation to the early Holocene. Geophys. Res. Lett. 30, 1001.
Seki, O., Meyers, P.A., Kawamura, K., Zheng, Y., Zhou, W., 2009a. Hydrogen isotopic ratios of plant wax n-alkanes in a peat bog deposited in northeast China during the last 16 kyr. Org. Geochem. 40, 671–677.
Seki, O., Mikami, Y., Nagao, S., Bendle, J.A., Nakatsuka, T., Kim, V.I., Shesterkin, V.P.,

Makinov, A.N., Fukushima, M., Moossen, H.M., Schouten, S., 2014. Lignin phenols and BIT index distributions in the Amur River and the Sea of Okhotsk: implications for the source and transport of particulate terrestrial organic matter to the ocean. Prog. Oceanogr. 126, 146–154.

Seki, O., Sakamoto, T., Sakai, S., Schouten, S., Hopmans, E.C., Damste, J.S.S., Pancost, R.D., 2009b. Large changes in seasonal sea ice distribution and productivity in the Sea of Okhotsk during the deglaciations. Geochem. Geophys. Geosys. 10, Q10007.

Serno, S., Winckler, G., Anderson, R.F., Maier, E., Ren, H., Gersonde, R., Haug, G.H., 2015. Comparing dust flux records from the Subarctic North Pacific and Greenland: implications for atmospheric transport to Greenland and for the application of dust as a chronostratigraphic tool. Paleoceanography 30, 583–600.

Shcherbina, A., Talley, L., Rudnick, D., 2004. Dense water formation on the northwestern shelf of the Okhotsk Sea: 1. Direct observations of brine rejection. J. Geophys. Res. Ocean 109, C09S08.

Shimizu, Y., Iwao, T., Yasuda, I., Ito, S., Watanabe, T., Uehara, K., Shikama, N., Nakano, T., 2004. Formation process of North Pacific intermediate water revealed by profiling floats set to drift on 26.7 sigma(theta) isopycnal surface. J. Oceanogr. 60, 453–462.

Southon, J., Noronha, A.L., Cheng, H., Edwards, R.L., Wang, Y., 2012. A high-resolution record of atmospheric 14C based on Hulu Cave speleothem H82. Quat. Sci. Rev. 33, 32–41.

Stuiver, M., Polach, H., 1977. Discussion: reporting of 14C data. Radiocarbon 19, 355–363.

Stuiver, M., Reimer, P.J., 1993. Extended 14C database and revised CALIB radiocarbon calibration program. Radiocarbon 35, 215–230.

Tachibana, Y., Oshima, K., Ogi, M., 2008. Seasonal and interannual variations of Amur River discharge and their relationships to large-scale atmospheric patterns and moisture fluxes. J. Geophys. Res. Atmos. 113, D16102.

Tadokoro, K., Ono, T., Yasuda, I., Osafune, S., Shiomoto, A., Sugisaki, H., 2009. Possible mechanisms of decadal-scale variation in PO 4concentration in the western North Pacific. Geophys. Res. Lett. 36, L08606.

Takahashi, T., Sutherland, S.C., Wanninkhof, R., Sweeney, C., Feely, R.A., Chipman, D.W., Hales, B., Friederich, G., Chavez, F., Sabine, C., Watson, A., Bakker, D.C.E., Schuster, U., Metzl, N., Yoshikawa-Inoue, H., Ishii, M., Midorikawa, T., Nojiri, Y., Körtzinger, A., Steinhoff, T., Hoppema, M., Olafsson, J., Arnarson, T.S., Tilbrook, B., Johannessen, T., Olsen, A., Bellerby, R., Wong, C.S., Delille, B., Bates, N.R., De Baar, H.J.W., 2009. Climatological mean and decadal change in surface ocean pCO2, and net sea–air CO2 flux over the global oceans. Deep Sea Res. Part II Top. Stud. Oceanogr. 56, 554–577.

Takeda, S., 2011. Iron and phytoplankton growth in the subarctic north Pacific. Aqua. BioSci. Monogr. 4, 41–93.

Talley, L.D., 1993. Distribution and formation of North Pacific intermediate water. J. Phys. Oceanogr. 23, 517–537.

Ternois, Y., Kawamura, K., Keigwin, L., Ohkouchi, N., Nakatsuka, T., 2001. A biomarker approach for assessing marine and terrigenous inputs to the sediments of Sea of Okhotsk for the last 27,000 years. Geochimica Cosmochimica Acta 65, 791–802.

Tjallingii, R., 2006. In: Wefer, G., Stein, R. (Eds.), Application and Quality of X-ray Fluorescence Core Scanning in Reconstructing Late Pleistocene NW African Continental Margin Sedimentation Patterns and Paleoclimate Variations. Fachbereich Geowissenschaften. Universität Bremen, Bremen, p. 114.

Uchimoto, K., Nakamura, T., Nishioka, J., Mitsudera, H., Misumi, K., Tsumune, D., Wakatsuchi, M., 2014. Simulation of high concentration of iron in dense shelf water in the Okhotsk Sea. Prog. Oceanogr. 126, 194–210.

Vaks, A., Gutareva, O.S., Breitenbach, S.F.M., Avirmed, E., Mason, A.J., Thomas, A.L., Osinzev, A.V., Kononov, A.M., Henderson, G.M., 2013. Speleothems reveal 500,000-year history of Siberian permafrost. Science 340, 183–186.

Van Geen, A., Zheng, Y., Bernhard, J., Cannariato, K., Carriquiry, J., Dean, W., Eakins, B., Ortiz, J., Pike, J., 2003. On the preservation of laminated sediments along the western margin of North America. Paleoceanography 18, 1098.

Verardo, D.J., Froelich, P.N., McIntyre, A., 1990. Determination of organic carbon and nitrogen in marine sediments using the Carlo Erba NA-1500 analyzer. Deep Sea Res. Part A. Oceanogr. Res. Pap. 37, 157–165.

Wang, Y., Cheng, H., Edwards, R., He, Y., Kong, X., An, Z., Wu, J., Kelly, M., Dykoski, C., Li, X., 2005. The Holocene Asian monsoon: links to solar changes and North Atlantic climate. Science 308, 854–857.

Wang, Y., Cheng, H., Edwards, R.L., Kong, X., Shao, X., Chen, S., Wu, J., Jiang, X., Wang, X., An, Z., 2008. Millennial- and orbital-scale changes in the East Asian monsoon over the past 224,000 years. Nature 451, 1090–1093.

Warren, B., 1983. Why is no deep water formed in the North Pacific? J. Mar. Res. 41, 327–347.

Watanabe, T., Wakatsuchi, M., 1998. formation of 26.8–26.9 $\sigma\theta$water in the Kuril basin of the sea of Okhotsk as a possible origin of north Pacific intermediate water. J. Geophys. Res. 103, 2849–2865.

Weltje, G.J., Tjallingii, R., 2008. Calibration of XRF core scanners for quantitative geochemical logging of sediment cores: theory and application. Earth Planet. Sci. Lett. 274, 423–438.

Wong, H., Ludmann, T., Baranov, B., Karp, B., Konerding, P., Ion, G., 2003. Bottom current-controlled sedimentation and mass wasting in the northwestern Sea of Okhotsk. Mar. Geol. 201, 287–305.

Yamamoto, M., Suemune, R., Oba, T., 2005. Equatorward shift of the subarctic boundary in the northwestern Pacific during the last deglaciation. Geophys. Res. Lett. 32, L05609.

Yamashita, Y., Cory, R.M., Nishioka, J., Kuma, K., Tanoue, E., Jaffé, R., 2010. Fluorescence characteristics of dissolved organic matter in the deep waters of the Okhotsk Sea and the northwestern North Pacific Ocean. Deep Sea Res. Part II Top. Stud. Oceanogr. 57, 1478–1485.

Yasuda, I., Okuda, K., Shimizu, Y., 1996. Distribution and modification of North Pacific intermediate water in the Kuroshio-Oyashio interfrontal zone. J. Phys. Oceanogr. 26, 448–465.

Yasuda, T., Asahara, Y., Ichikawa, R., Nakatsuka, T., Minami, H., Nagao, S., 2014. Distribution and transport processes of lithogenic material from the Amur River revealed by the Sr and Nd isotope ratios of sediments from the Sea of Okhotsk. Prog. Oceanogr. 126, 155–167.

Yoshikawa, C., Nakatsuka, T., Wakatsuchi, M., 2006. Distribution of N* in the Sea of Okhotsk and its use as a biogeochemical tracer of the Okhotsk Sea intermediate water formation process. J. Mar. Syst. 63, 49–62.

Zheng, Y., Van Geen, A., Anderson, R., Gardner, J., Dean, W., 2000. Intensification of the northeast Pacific oxygen minimum zone during the Bolling-Allerod warm period. Paleoceanography 15, 528–536.